SIAM J. APPLIED DYNAMICAL SYSTEMS
Vol. 2, No. 1, pp. 1–35

The Forced van der Pol Equation I: The Slow Flow and Its Bifurcations*

John Guckenheimer†, Kathleen Hoffman‡, and Warren Weckesser§

Abstract. The forced van der Pol oscillator has been the focus of scientific scrutiny for almost a century, yet its global bifurcation structure is still poorly understood. In this paper, we present a hybrid system consisting of the dynamics of the trajectories on the slow manifold coupled with "jumps" at the folds in the critical manifold to approximate the fast subsystem. The global bifurcations of the fixed points and periodic points of this hybrid system lead to an understanding of the bifurcations in the periodic orbits (without canards) of the forced van der Pol system.

Key words. van der Pol oscillator, hybrid dynamical system, bifurcations, chaotic attractor, periodic solutions

AMS subject classifications. 37C10, 37C27, 37G15

PII. S1111111102404738

1. Introduction.

During the first half of the twentieth century, Balthazar van der Pol pioneered the fields of radio and telecommunications [6, 7, 29, 32, 33, 34]. In an era when these areas were much less advanced than they are today, vacuum tubes were used to control the flow of electricity in the circuitry of transmitters and receivers. Contemporary with Lorenz, Thompson, and Appleton, van der Pol experimented with oscillations in a vacuum tube triode circuit and concluded that all initial conditions converged to the same periodic orbit of finite amplitude. Since this behavior is different from the behavior of solutions of linear equations, van der Pol proposed a nonlinear differential equation

$$x'' + \mu(x^2 - 1)x' + x = 0, \tag{1.1}$$

commonly referred to as the (unforced) van der Pol equation [32], as a model for the behavior observed in the experiment. In studying the case $\mu \gg 1$, van der Pol discovered the importance of what has become known as *relaxation oscillations* [33]. These oscillations have become the cornerstone of geometric singular perturbation theory and play a significant role in the analysis presented here. Van der Pol went on to propose a version of (1.1) that includes a periodic forcing term:

$$x'' + \mu(x^2 - 1)x' + x = a\sin(2\pi\nu\tau). \tag{1.2}$$

In a similar equation, he and van der Mark first noted the existence of two stable periodic solutions with different periods for a particular value of the parameters and observed noisy

*Received by the editors April 1, 2002; accepted for publication (in revised form) by M. Golubitsky September 24, 2002; published electronically February 19, 2003.
http://www.siam.org/journals/siads/2-1/40473.html

†Mathematics Department, Cornell University, Ithaca, NY 14853 (gucken@com.cornell.edu).
‡Department of Mathematics and Statistics, University of Maryland, Baltimore County, Baltimore, MD 21250 (khoffman@math.umbc.edu).
§Mathematics Department, Colgate University, Hamilton, NY 13346 (wweckesser@mail.colgate.edu).

behavior in an electrical circuit modeled with (1.2) [35]. Van der Pol further speculated that (1.2) also had this property.

Van der Pol's work on nonlinear oscillations and circuit theory provided motivation for the seminal work of Cartwright and Littlewood [22]. In 1938, just prior to World War II, the British Radio Research Board issued a request for mathematicians to consider the differential equations that arise in radio engineering. Responding to this request, Cartwright and Littlewood began studying the forced van der Pol equation and showed that it does indeed have bistable parameter regimes. In addition, they showed that there does not exist a smooth boundary between the basins of attraction of the stable periodic orbits. They discovered what is now called chaotic dynamics by detailed investigation of this system [7, 8, 9, 20, 21].

Since its introduction in the 1920's, the van der Pol equation has been a prototype for systems with self-excited limit cycle oscillations. The equation has been studied over wide parameter regimes, from perturbations of harmonic motion to relaxation oscillations. It has been used by scientists to model a variety of physical and biological phenomena. For instance, in biology, the van der Pol equation has been used as the basis of a model of coupled neurons in the gastric mill circuit of the stomatogastric ganglion [15, 26]. The Fitzhugh–Nagumo equation [12] is a planar vector field that extends the van der Pol equation as a model for action potentials of neurons [18]. In seismology, the van der Pol equation has been used in the development a model of the interaction of two plates in a geological fault [5].

Despite the continuing work of many scientists and mathematicians (see [13, 16, 17, 19, 26, 28, 30, 31], for example), bifurcations of this system have been studied little. This paper is the first in a series that seeks to give a thorough analysis of the dynamics inherent in the forced van der Pol equation in the relaxation regime. Here we focus upon a two-dimensional reduced system derived from the forced van der Pol equation, classifying the bifurcations of the simplest periodic orbits in this reduced system.

2. Fast subsystems and the slow flow. We begin by setting notation and defining the fast subsystems and slow flow of the forced van der Pol equation. First, we change variables to express (1.2) in a more convenient form by rescaling time $t = \tau/\mu$, so $x' \to \dot{x}/\mu$ and $x'' \to \ddot{x}/\mu^2$, where $\dot{x} \equiv dx/dt$. By defining $y = \dot{x}/\mu^2 + x^3/3 - x$, we transform (1.2) into the system

$$\begin{aligned} \frac{1}{\mu^2}\dot{x} &= y - \frac{x^3}{3} + x, \\ \dot{y} &= -x + a\sin(2\pi\nu\mu t). \end{aligned}$$

Defining new parameters $\varepsilon = 1/\mu^2$ and $\omega = \nu\mu$ and converting these equations into an autonomous system by defining $\theta = \omega t$, we obtain the system

$$\begin{aligned} \varepsilon\dot{x} &= y + x - \frac{x^3}{3}, \\ \dot{y} &= -x + a\sin(2\pi\theta), \\ \dot{\theta} &= \omega \end{aligned} \tag{2.1}$$

as a vector field on $\mathbb{R}^2 \times S^1$. We regard $S^1 = \mathbb{R}/\mathbb{Z}$ and use coordinates $[0, 1]$ for S^1, understanding that the endpoints are identified. We also use the system in the form

$$\begin{aligned} \frac{dx}{ds} &= y + x - \frac{x^3}{3}, \\ \frac{dy}{ds} &= \varepsilon(-x + a\sin(2\pi\theta)), \\ \frac{d\theta}{ds} &= \varepsilon\omega, \end{aligned} \tag{2.2}$$

obtained by rescaling time by $s = \varepsilon t$. In the relaxation regime, namely, $\varepsilon \ll 1$, these equations can be analyzed using singular perturbation theory [14]. The variable x is commonly referred to as the *fast variable*, and the variables y and θ are the *slow variables*. Exploiting the two time scales in (2.1) and (2.2), trajectories are decomposed into fast and slow segments. This decomposition is achieved by considering the dynamics of the singular limit $\varepsilon = 0$ in (2.1) and (2.2).

The limit $\varepsilon = 0$ in (2.2) results in the family of *fast subsystems*. For each y and θ, the fast subsystem is a one-dimensional differential equation for x, with y and θ acting as parameters. If $|y| > 2/3$, there is a single stable equilibrium, and if $|y| < 2/3$, there are two stable and one unstable equilibria of the fast subsystem. The forward limit of each trajectory is one of the stable equilibria. The singular limit $\varepsilon = 0$ of (2.1) results in a differential algebraic equation. The first equation in (2.1) becomes $y = x^3/3 - x$, which defines a two-dimensional manifold called the *critical manifold*. The critical manifold is the union of equilibria of the fast subsystems. The remaining two equations of (2.1) define implicitly a vector field on the critical manifold at regular points of its projection onto the (y, θ) coordinate plane. This vector field on the critical manifold is called the *slow flow* of the system. We call the pieces of the critical manifold composed of stable equilibria of the fast subsystems the *stable sheets* (there are two disjoint stable sheets—one where $x > 1$ and one where $x < 1$), and we call the piece composed of unstable equilibria the *unstable sheet* (where $|x| < 1$).

The relationship between the full system ($\varepsilon \neq 0$, (2.1)) and the slow flow was studied by Tikhonov [2, 24] and later by Fenichel [11]. Fenichel proved that there exists a *slow manifold*, that is, an invariant manifold, within distance $O(\varepsilon)$ of the critical manifold on compact regions of regular points. Moreover, the slow flow on the critical manifold gives $O(\varepsilon)$ approximations to trajectories of the forced van der Pol equation.

For $\varepsilon \neq 0$, systems (2.1) and (2.2) are equivalent, but the limit systems as $\varepsilon \to 0$ are quite different. The trajectories of (2.1) consist of segments for which the fast subsystem is a good approximation to the dynamics and segments for which the slow subsystem is a good approximation to the dynamics. The transitions between these segments occur at folds. Folds are the singular points of the projection of the critical manifold onto the (y, θ) plane. For the forced van der Pol equation, these folds occur at $x = \pm 1, y = \mp 2/3$. As $\varepsilon \to 0$, many solutions of the full system approach curves that are concatenations of trajectories of the slow flow and trajectories of the fast subsystem, joined at fold points of the critical manifold.

Figure 2.1 shows a trajectory of the full system ((2.1), $\varepsilon \neq 0$) along with the critical manifold and the slow flow on that manifold. This figure illustrates the roles of the fast subsystems and slow flow in understanding solutions to the full system. The yellow curve is a

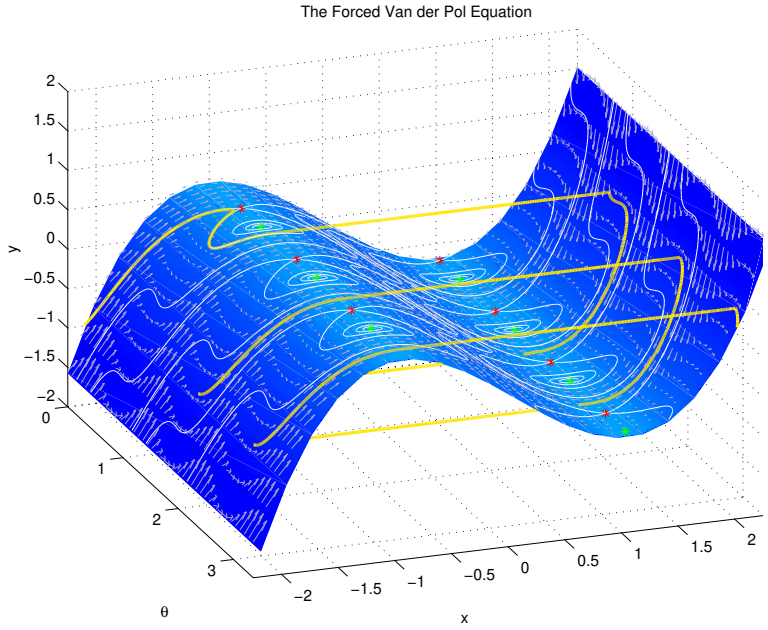

Figure 2.1. *The two-dimensional surface illustrates the critical manifold of the forced van der Pol equations* (2.1)*. In this example,* $a = 2.3$ *and* $\omega = 1$*. The white arrows are the vector field of the slow flow on the critical manifold, and the white curves are corresponding trajectories of that vector field. The green and red asterisks located at the folds of the critical manifold are the folded singularities, foci and saddles, respectively. The yellow curve represents a solution to* (2.1) *for* $\varepsilon = 10^{-4}$*.*

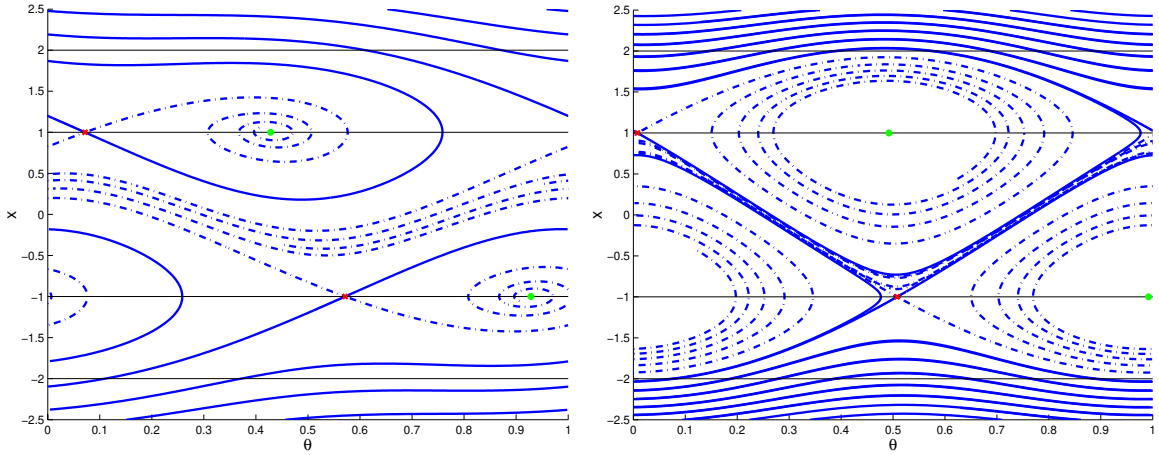

(a) (b)

Figure 2.2. *These are examples of the slow flow. In* (a)*, the parameters are* $a = 2.3$ *and* $\omega = 1$*, the same as in Figure* 2.1*. In* (b)*,* $a = 20$ *and* $\omega = 5$*, which are the same values shown in Figures* 4.1(a) *and* 4.2*. The plots show the stable and unstable manifolds of the folded saddles, along with the circles* $x = \pm 1$ *and* $x = \pm 2$*.*

solution to the full system (2.1), with $\varepsilon = 10^{-4}$, $a = 2.3$, and $\omega = 1$. The blue two-dimensional surface is the critical manifold, and the white curves and arrows show the trajectories of the slow flow and its vector field on the critical manifold, respectively. Notice that the solution to the full system appears to follow the slow flow until it reaches a fold in the critical manifold, where it then appears to follow the fast subsystem until again reaching the critical manifold. The red and green asterisks mark *folded singularities*, points on the fold curves of the critical manifold that play a central role in our analysis of bifurcations. Figure 2.2 gives examples of the slow flow for two sets of parameter values. The folds of the critical manifold are the lines $x = \pm 1$, and the "landing points" of the jumps from the folds (that is, the projections of the fold lines along the fast variable onto the critical manifold) are the lines $x = \pm 2$.

The next section defines a reduced hybrid system whose solutions come from piecewise smooth curves that approximate solutions of the system (2.1) and consist of segments that are solutions to the fast subsystems and slow flow.

3. The reduced system. The main idea of this paper is to study the global bifurcations of the forced van der Pol equation by studying a *reduced system* Ψ_h, a hybrid dynamical system that combines solutions to the slow flow of (2.1) with discrete time transformations along trajectories of the fast subsystems. Specifically, the reduced system is defined to follow the slow flow on the stable sheets $|x| \geq 1$ of the critical manifold and to have discrete time jumps from $(\theta, \pm 1)$ to $(\theta, \mp 2)$ on the boundaries of the two stable sheets. The boundaries of the two stable sheets are *folds* of the projection of the critical manifold (see Figure 2.1) onto the two-dimensional space of slow variables. Trajectories of the system Ψ_h give approximations to many trajectories of the full three-dimensional flow. We explain the nature of this approximation in section 4.

The projection $\pi(x, y, \theta) = (y, \theta)$ of the critical manifold onto the (θ, y) space of slow variables is singular on the *fold* curves $x = \pm 1, y = \mp 2/3$. Due to these singularities, we use (θ, x) as coordinates for the slow flow, with (θ, x) lying in one of the two closed half-cylinders $x \geq 1$ or $x \leq 1$. We reparametrize the slow flow to obtain the vector field

$$\begin{aligned} \theta' &= \omega(x^2 - 1), \\ x' &= -x + a\sin(2\pi\theta). \end{aligned} \tag{3.1}$$

The vector field (3.1) is obtained from the forced van der Pol equation (2.1) by differentiating the algebraic equation $y = x^3/3 - x$ to obtain $\dot{y} = (x^2 - 1)\dot{x}$, substituting the result into the van der Pol equation (2.1), and rescaling the time by $(x^2 - 1)$. We shall henceforth call the system (3.1) the slow flow since it has the same trajectories as the original slow flow on the stable sheets of the critical manifold. However, there are several ways in which this rescaled system (3.1) differs from the slow flow in its original coordinates. First, it is defined on the fold curves, while the original equations are not due to the singularity of the projection π. Second, it reverses time on the unstable sheet, represented by the cylinder $|x| < 1$ in the (θ, x) coordinates. Therefore, the direction of the slow flow on the unstable sheet of the critical manifold is opposite that defined by (3.1). Note that the system (3.1) has equilibrium points on the circles $x = \pm 1$ if $a \geq 1$. These equilibria are called *folded equilibria*. They approximate points where the flow of the van der Pol equation (2.1) is tangent to the fold curves. The van der Pol equation (2.1) has no equilibria.

We establish a few basic properties of the slow flow. If $x > a > 0$, then $x' < 0$, while if $x < -a < 0$, then $x' > 0$. Consequently, the region $|x| < a$ is forward invariant for system (3.1), and all trajectories flow into this region. The vector field is symmetric with respect to the symmetry given by $T(\theta, x) = (\theta + \frac{1}{2}, -x)$. We also observe that the divergence of the vector field is constant, namely, -1. Therefore, its flow can have at most a single periodic orbit. Periodic orbits must be T-symmetric (otherwise, there would be a symmetric partner) and consequently cross $x = 0$. The equilibrium points of the slow flow lie on the circles $x = \pm 1$. We conclude that all trajectories with initial conditions satisfying $|x| > 1$ reach the circles $x = \pm 1$ unless they lie in the stable manifold of an equilibrium point, in which case they approach $x = \pm 1$ as $t \to \infty$.

The equilibrium points of the slow flow lie at the points $(\theta, x) = (\pm \sin^{-1}(1/a)/2\pi, \pm 1)$. Here $\sin^{-1}$ is regarded to be a double valued "function" on $(-1, 1)$. If $a = 1$, there are two equilibrium points; if $a > 1$, there are four equilibrium points. The linear stability of the equilibria is easily computed [28] using the Jacobian of the slow flow equations:

$$\begin{pmatrix} -1 & 2\pi a \cos(2\pi\theta) \\ 2\omega x & 0 \end{pmatrix}.$$

At $a = 1$, the equilibria are saddle-nodes. For $a > 1$, two of the equilibria are saddles. In the parameter interval $1 < a < \sqrt{1 + 1/(16\pi\omega)^2}$, the two remaining equilibria are stable nodes. When $a = \sqrt{1 + 1/(16\pi\omega)^2}$, these equilibria are resonant with a single negative eigenvalue, and when $a > \sqrt{1 + 1/(16\pi\omega)^2}$, they are stable foci. We see below that some global bifurcations of Ψ_h depend upon the type of stable equilibrium points found in the slow flow.

We label the coordinates of the saddle point on $x = 1$ as $(\theta, x) = (\theta_{1s}, 1)$ and the coordinates of the node as $(\theta_{1n}, 1)$. The unstable and stable manifolds of the saddle will be denoted by the standard notation W_u and W_s, respectively. We further define the point $p_{1u} = (\theta_{1u}, 1)$ to be the first intersection of the unstable manifold W_u of $(\theta_{1s}, 1)$ with $x = 1$ and set θ_{2si} to be the θ coordinate of the ith intersection of the stable manifold W_s of the saddle $(\theta_{1s}, 1)$ with $x = 2$ as W_s is traversed backward from $x = 1$ into the region $x > 1$. This notation will be used in our description of the properties of the hybrid system Ψ_h and its bifurcations. Figure 4.1 displays phase portraits of the slow flow for two sets of parameter values.

4. Return maps. When $\varepsilon > 0$ is small, trajectories of the van der Pol equation (2.1) with initial conditions near the stable sheets of the critical manifold that do not pass close to the folded singularities are approximated by trajectories of the reduced system Ψ_h [19]. Consequently, bifurcations of the reduced system identify the location of parameters at which bifurcations of the van der Pol equation are expected. Our primary goal in this paper is to identify bifurcations of the reduced system Ψ_h. (Later papers in this series will investigate the relationship between bifurcations of Ψ_h and those of the van der Pol equation (2.1).) In this section, we develop and describe a return map from the circle S_2 (defined by the equation $x = 2$) to itself as a means of describing periodic solutions to the hybrid system Ψ_h.

4.1. Derivation of the half-return map H. Using the observations in the last section, we define two maps $P_\pm$ along trajectories from the circles $S_{\pm 2}$ defined by $x = \pm 2$ to the circles $S_{\pm 1}$ defined by $x = \pm 1$. At points that are not in the stable manifolds of the equilibria, the maps $P_\pm$ are well defined and smooth. At transverse intersections of the stable manifolds of

the saddles with $S_{\pm 2}$, the maps $P_\pm$ are discontinuous. At the circles $x = \pm 1$ on the critical manifold, trajectories of the forced van der Pol equation jump from a fold to the circles $x = \mp 2$ on the critical manifold. For the two-dimensional reduced system, we define the operators $J_+(\theta, 1) = (\theta, -2)$ and $J_-(\theta, -1) = (\theta, 2)$ that describe the discrete jumps in Ψ_h. The return map for Ψ_h to the circle S_2 is then given by the composition $J_-P_-J_+P_+$ since

$$\begin{aligned} P_+ &: S_2 \to S_1, \\ J_+ &: S_1 \to S_{-2}, \\ P_- &: S_{-2} \to S_{-1}, \\ J_- &: S_{-1} \to S_2. \end{aligned}$$

Actually, the map $J_-P_-J_+P_+$ is the perfect square of a half-return map H. To define H, we use the symmetry operator $T(\theta, x) = (\theta + \frac{1}{2}, -x)$. We note that the slow flow and the reduced system Ψ_h are symmetric with respect to the transformation T, T^2 is the identity on $S^1 \times \mathbb{R}$, and the following relations hold: $TP_+ = P_-T$ and $TJ_+ = J_-T$. Then the return map $J_-P_-J_+P_+ = J_-P_-TTJ_+P_+ = (TJ_+P_+)(TJ_+P_+)$ is the square of the map $H = (TJ_+P_+)$ on the circle S_2. Consequently, the periodic orbits of Ψ_h can be divided into those that are fixed by the half-return map H and those that are not. Because T phase shifts θ by $\frac{1}{2}$, the fixed points of H all yield T-symmetric periodic orbits that make exactly two jumps—one from $x = 1$ to $x = -2$ and one from $x = -1$ to $x = 2$. In this paper, we study the bifurcations of periodic orbits of the reduced system Ψ_h with a focus upon fixed points and period 2 points of the half-return map H. These bifurcations correspond to bifurcations of periodic orbits in the forced van der Pol oscillator that are T-symmetric and have just two jumps. The stable periodic orbits studied by Cartwright and Littlewood [9, 20, 21] are in this class: they are T-symmetric with two jumps and yield fixed points of H.

4.2. Properties of H. The half-return map H depends on the two parameters a and ω. The lines $a = 1$ and $a = 2$ divide the a-ω plane into regions in which H has fundamentally different properties. The map P_+ is a diffeomorphism of the circle S_2 to the circle S_1 for $0 < a < 1$. In this regime, x decreases along all trajectories in the strip $1 < x < 2$, implying that H is a circle diffeomorphism. Its rotation number depends upon ω, increasing with ω. All rotation numbers in $[\frac{1}{2}, \infty)$ are realized as ω varies in $(0, \infty)$.

When $1 < a < 2$, the map P_+ no longer maps the circle S_2 onto the circle S_1. Its image I_1 excludes the portion of S_1 that lies below the unstable manifold W_u defined in the previous section. The discontinuities in the domain of P_+ occur at points in $W_s \cap S_2$. There is a single point of discontinuity since the circle S_2 is a cross-section for the flow and W_s crosses S_2 only once. It also follows that the map P_+ remains increasing in this parameter regime. Thus H is a family of increasing maps of the circle into itself with a single point of jump discontinuity in this parameter regime. This implies that H still has a well-defined rotation number, and the period of all of its periodic orbits is the denominator of the rotation number. Quasi-periodic trajectories are still possible, but the set of parameter values yielding quasi-periodic trajectories is likely to have measure zero [16].

When $2 < a$, the map P_+ is no longer monotone. There are two points $p_{2l} = (\theta_{2l}, 2) = (\frac{1}{2\pi}\sin^{-1}(\frac{2}{a}), 2)$ and $p_{2r} = (\theta_{2r}, 2) = (\frac{1}{2} - \frac{1}{2\pi}\sin^{-1}(\frac{2}{a}), 2)$ at which P_+ has a local maximum

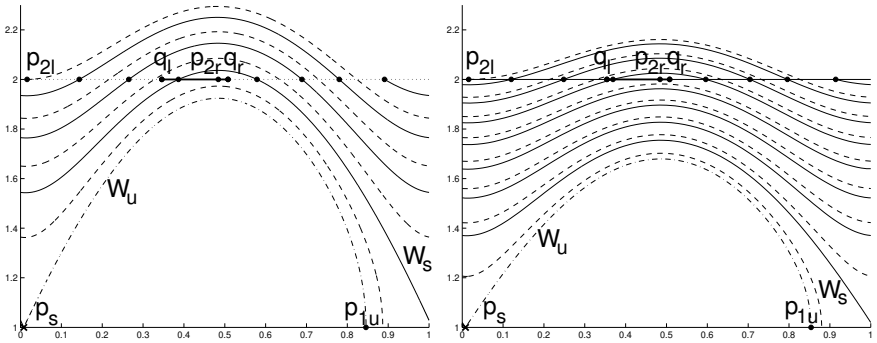

Figure 4.1. *The structure of the reduced system in the half-cylinder* $1 < x$ *for* (a) $(\omega, a) = (5, 20)$ *and* (b) $(\omega, a) = (10, 20)$. *Unstable manifolds* W_u *are drawn with dot-dash curves, stable manifolds* W_s *are drawn solid, the trajectories originating at the points* p_{2l} *are drawn dashed, and the circles* $x = 2$ *are drawn as dotted lines.*

and minimum, respectively. On the interval $D = (\theta_{2l}, \theta_{2r})$, P_+ has negative slope, while on $S^1 - \bar{D}$, it has positive slope. There are two crucial additional aspects to the structure of H as a piecewise continuous and piecewise monotone mapping of the circle. First, there are discontinuities of P_+ at intersections of D with W_s. (There may be only one such intersection point.) At the points of discontinuity in $W_s \cap S_2$, there is a jump with limit values $\frac{1}{2} + \theta_{1s} = \theta_r$ and $\frac{1}{2} + \theta_{1u} = \theta_l$. We denote by q_l and q_r the points $(\theta_l, 2)$ and $(\theta_r, 2)$ in S_2. Second, we observe that the maximum height of W_u is a decreasing function of ω and is unbounded as $\omega \to 0$. Therefore, if $\omega > 0$ is small enough, W_u intersects the circle S_2. When this happens, it divides S_2 into two intervals. The points in S_2 above W_u have their images in $I_H = [q_l, q_r]$, while the points in S_2 below W_u have their images to the left of q_l. (If $0 < \theta_{1s} < \frac{1}{2} < \theta_{1u} < 1$, then $I_H \subset [0, 1]$. Otherwise, if $0 < \theta_{1u} < \frac{1}{2}$, the circular arc I_H contains 0, and it is convenient to choose a fundamental domain for the universal cover of the circle S_2 that contains $[q_l, q_r]$.) Note that W_s lies above W_u.

Figure 4.1 shows the structure of the flow in the strip $1 < x < 2.25$ for $a = 20$, with $\omega = 5$ on the left and $\omega = 10$ on the right. (Note that $\theta = 0$ and $\theta = 1$ are identified, so the flow is actually on a cylinder: $(\theta, x) \in S^1 \times \mathbb{R}$.) The folded saddles p_s are located by the symbol $\times$. Their stable separatrices are drawn as solid curves, and their unstable manifolds are drawn as dot-dashed curves. The circles S_2 are drawn dotted, and the points p_{2l} and p_{2r} are labeled. The dashed trajectories have initial condition p_{2l}. The intervals $I_H = [q_l, q_r]$ that are the images of most branches of H are drawn as thick lines. The points $p_{1u} \in W_u \cap S_1$ are labeled, and the points in $W_s \cap S_2$ are marked by large dots. The graph of the half-return map H for $(\omega, a) = (5, 20)$ is shown in Figure 4.2. The map H is discontinuous at the points of $W_s \cap S_2$ and has a local maximum at p_{2l} and a local minimum at p_{2r}.

The topological theory of one-dimensional maps is based upon partitioning the domain of a map into intervals on which it is continuous and monotone. Here the graph of H can contain the following types of intervals on which it is continuous and monotone:

- a decreasing branch with domain $[p_{2l}, p_{2r}]$ (this occurs if $a > 2$ but W_s intersects S_2 in a single point),

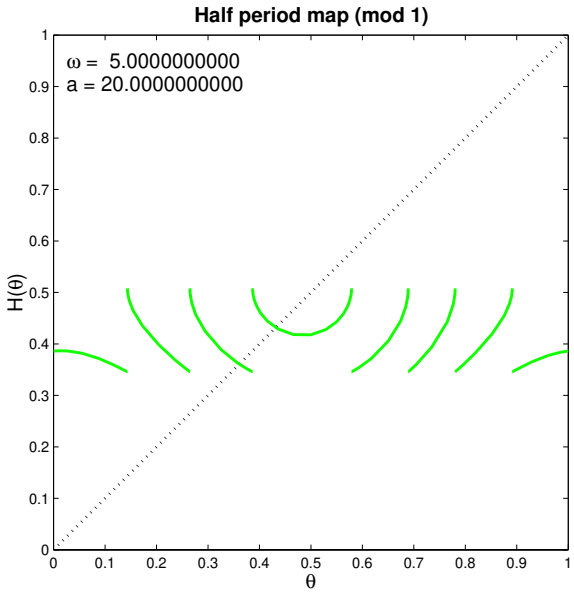

Figure 4.2. *The graph of H when $a = 20$ and $\omega = 5$. These are the same parameter values as in Figure 4.1(a). Note that the discontinuities of H occur at the intersections of W_s with S_2, and H has a local maximum and a local minimum at the θ coordinates of p_{2l} and p_{2r}, respectively.*

- a branch containing p_{2r} with a local minimum,
- a branch containing p_{2l} with a local maximum,
- monotone decreasing branches in (p_{2l}, p_{2r}),
- monotone increasing branches in the complement of $[p_{2l}, p_{2r}]$.

We assume for the moment that all intersections of W_s with S_2 are transverse. Then W_s must have an odd number of intersections with S_2, and every intersection in $[\theta_{2l}, \theta_{2r}]$ is preceded by an intersection in the complement of this interval. Therefore, the number of monotone increasing branches is one larger than the number of monotone decreasing branches. Moreover, the image of all branches is contained in I_H with the possible exception of the branch with a local minimum. The branch structure of H will play an important role in defining the different types of bifurcations in section 5. In particular, saddle-node bifurcations will occur on the branch with a local minimum, and homoclinic points occur at the endpoints of certain branches.

The local maximum and minimum of H occur at points where the vector field is tangent to the circle $x = 2$. The circles $x = \pm 2$ are the images of the fold curves $x = \mp 1$ in the reduced system. Differentiating the equation $x' = -x + a\sin(2\pi\theta)$, we obtain $x'' = -x' + \frac{a}{2\pi}\cos(2\pi\theta)\theta' = \frac{3a\omega}{2\pi}\cos(2\pi\theta) \neq 0$ since $x' = 0$ and $|\sin(2\pi\theta)| < 1$. Therefore, the curvature of the trajectories is not zero at the tangencies with $x = 2$, and there are local extrema for H at these points.

Next we analyze the points of discontinuity for the map H. The end of a branch behaves quite differently depending upon whether the trajectories of points near the end of the branch of H lie to the left or right of the stable manifold W_s of the saddle and upon whether there is

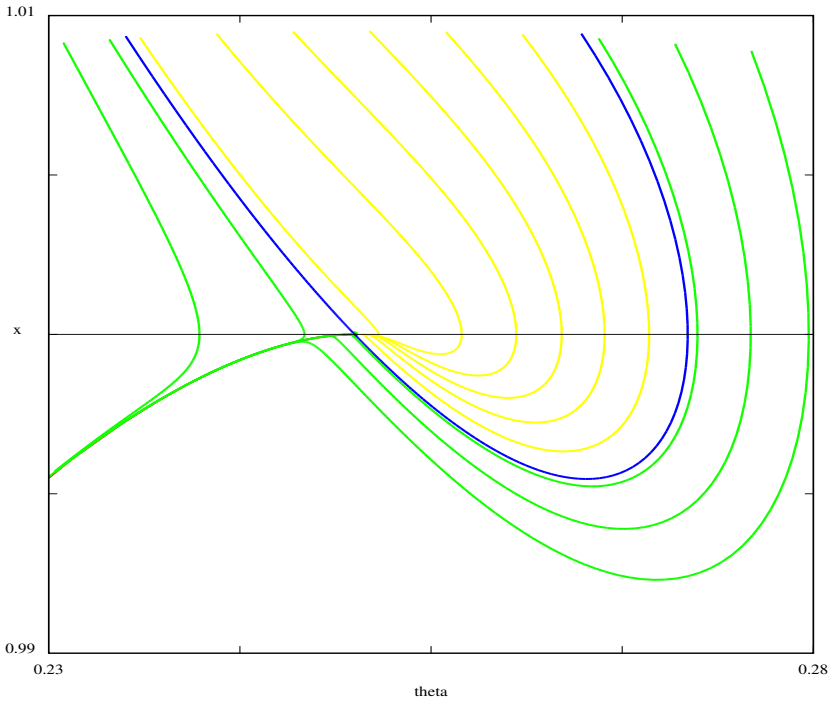

Figure 4.3. *The flow of Ψ_h near a saddle-node. Trajectories in the strong stable manifold are drawn in blue, trajectories in the interior of the stable manifold are drawn in yellow, and trajectories in the hyperbolic region are drawn in green.*

a folded node or a folded focus. In the case in which the trajectories lie to the left of W_s, they cross the circle $x = 1$ immediately to the left of the saddle. We give an asymptotic analysis of the slope of H at the branch end by approximating the flow near the saddle by a linear flow. Introducing coordinates for which the linear unstable and stable manifolds of the saddle are the u and v axes respectively, the linear approximation of the slow flow is

$$\begin{aligned} u' &= \alpha u, \\ v' &= -\beta v \end{aligned} \tag{4.1}$$

with $0 < \alpha$ and $\beta = \alpha+1$ since the trace of the Jacobian at the saddle is -1. The function $u^\beta v^\alpha$ is constant along trajectories of system (4.1). In these coordinates, the circle $x = 1$ becomes a line of the form $v = cu$. The flow from any cross-section to the stable manifold along the v axis to this line will have a derivative that becomes infinite. For example, the intersection (u_1, v_1) of the trajectory through $(u_0, 1)$ with this line will satisfy $|u_0|^\beta = |u_1|^\beta |v_1|^\alpha$ and $|u_1| = |c|^{-\alpha/(\alpha+\beta)} |u_0|^{\beta/(\alpha+\beta)}$. Since $\beta/(\alpha+\beta) < 1$, the slope of this function tends to infinity as $u_0 \to 0$. This argument implies that the slope of H is unbounded for points to the left of W_s.

In the case in which trajectories at the end of the branch pass to the right of W_s, they proceed along the unstable manifold W_u before they cross the circle $x = 1$. If there is a folded

Table 5.1
A summary of the types of bifurcations and their defining equations.

Type of bifurcation	Defining equation
Saddle-node	$H(x) = x,\ H'(x) = 1$
Saddle left homoclinic	$\theta_{2s1} - \theta_{1s} - 0.5 = 0 \pmod 1$
Saddle right homoclinic 1	$\theta_{2s1} - \theta_{1u} - 0.5 = 0 \pmod 1$
Saddle right homoclinic 2	$\theta_{2s2} - \theta_{1u} - 0.5 = 0 \pmod 1$
Saddle right homoclinic 3	$\theta_{2s3} - \theta_{1u} - 0.5 = 0 \pmod 1$
Nodal homoclinic	$\theta_{2ss1} - \theta_{1n} - 0.5 = 0 \pmod 1$
Heteroclinic	$\theta_{1n} - \theta_{2s1} - 0.5 = 0 \pmod 1$

focus, they cross $x = 1$ to the right of W_u. If there is a folded node, these trajectories tend to the node. In the case of the focus, it is well known that the mapping from a cross-section to W_s to a cross-section to W_u will behave asymptotically like $u^{\beta/\alpha}$ at its endpoint. Since $\beta/\alpha > 1$, the derivative approaches 0 as u tends to 0. We conclude that at points of discontinuity for H, the slope is unbounded on one side of the discontinuity (the side of trajectories to the left of W_s), and the slope approaches zero on the opposite side (the side of trajectories to the right of W_s). In the case of a folded node, the half-return map H is undefined on the interval of points between W_s and the strong stable manifold of the node. We choose to extend H to this interval, giving it the constant value that is its limit as points approach the strong stable manifold of the node from the right. See Figure 4.3.

Our analysis of bifurcations will make substantial use of one additional concept that we call the *circuit number* of a trajectory for the reduced system and for H. We lift the slow flow to the universal cover of $\mathbb{R} \times S^1$, and consider trajectories that flow from $(\theta_0, 2)$ to $(\theta_1, 1)$ on the universal cover. The integer part of $\theta_1 - \theta_0$ will be called the circuit number of the trajectory. As ω increases, θ' increases, and the circuit number of the trajectories increase. This leads to a repetitive structure in the bifurcation diagram for the reduced system, in which the same structures reappear in the parameter space, once for each circuit number.

5. Codimension one bifurcations of fixed points.

5.1. Bifurcation types and defining equations. This section characterizes the codimension one bifurcations of fixed points that we find for the half-return map H. We have found at most three fixed points for any parameter value. These fixed points are confined to two branches of H: the branch containing a local minimum and the branch immediately to the left of the branch containing a local minimum. We have not proved that these are the only possible locations of fixed points, but this is consistent with the bifurcation diagram described in section 5.2. Codimension one bifurcations of fixed points for H fall into three classes:

- saddle-node bifurcations,
- homoclinic bifurcations, and
- heteroclinic bifurcations.

For the first two types of bifurcations, we make further distinctions, described in sections 5.1.1 and 5.1.2. Table 5.1 contains a summary of the bifurcations and their defining equations that will be described in the next sections.

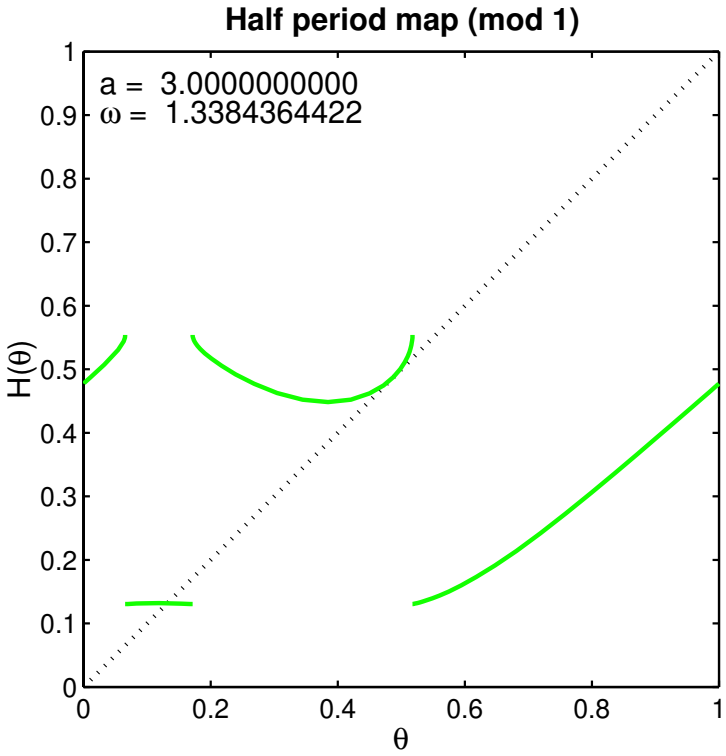

Figure 5.1. *The graph of the half-return map for the given values of a and ω shows a min saddle-node bifurcation, as can be seen by the tangency of the third branch of H with the dotted line $H(\theta) = \theta$ at a minimum of $H - I$.*

5.1.1. Saddle-node bifurcations. The saddle-nodes are distinguished by whether $H - I$ has a local minimum or maximum at the saddle-node point. We call these min and max saddle-nodes, respectively. Figure 5.1 is an example of a min saddle-node, and Figure 5.2 is an example of a max saddle-node. The defining equations for saddle-node bifurcations are $H(x) = x$ together with $H'(x) = 1$.

5.1.2. Homoclinic bifurcations. We distinguish two types of homoclinic orbits—those with a homoclinic connection to the folded saddle, called *saddle homoclinic orbits* and those with a homoclinic connection to the folded node along its strong stable manifold, called *nodal homoclinic orbits*. We further classify the saddle homoclinic orbits as *left homoclinic* or *right homoclinic*, depending on whether the orbit is the limit of trajectories lying to the left or to the right of the stable manifold of the saddle.

The defining equation for a left homoclinic bifurcation is $\theta_{2s1} - \theta_{1s} - 0.5 = 0 \pmod 1$, which guarantees that the first intersection of the stable manifold of the saddle with $x = 2$, namely, θ_{2s1}, is the image of θ_{1s} under TJ_+ (see Figure 5.3). Thus a saddle left homoclinic orbit flows from $(\theta_{2s1}, 2)$ to the saddle (in infinite time) and then is mapped back to its starting point by TJ_+. Fixed points near a left homoclinic saddle bifurcation leave $x = 1$ to the left of the folded saddle point $(\theta_{1s}, 1)$ and return to $x = 2$ near the stable manifold of the folded

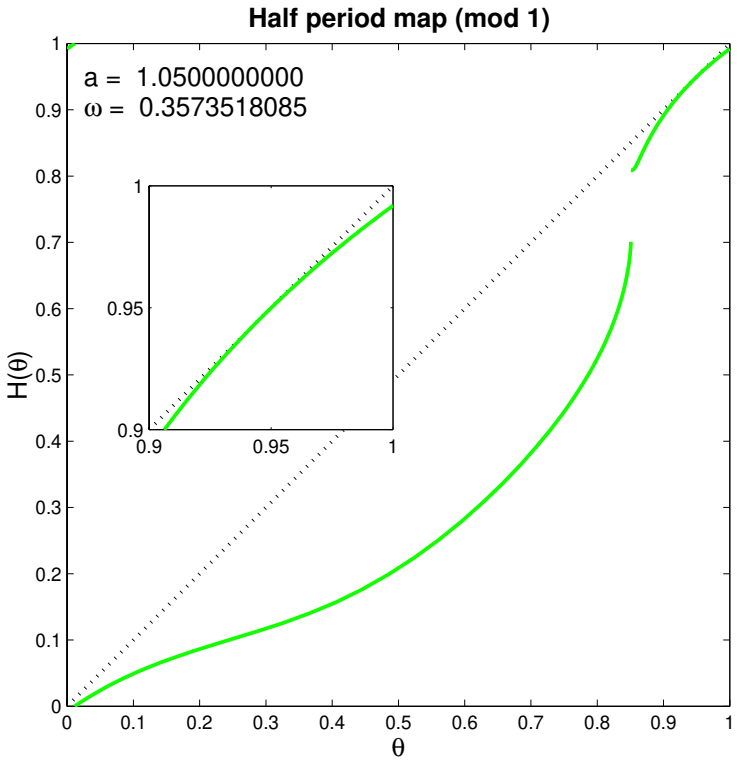

Figure 5.2. *The graph of the half-return map for the given values of a and ω shows a max saddle-node bifurcation, as can be seen by the tangency of the third branch of H with the dotted line $H(\theta) = \theta$ at a maximum of $H - I$.*

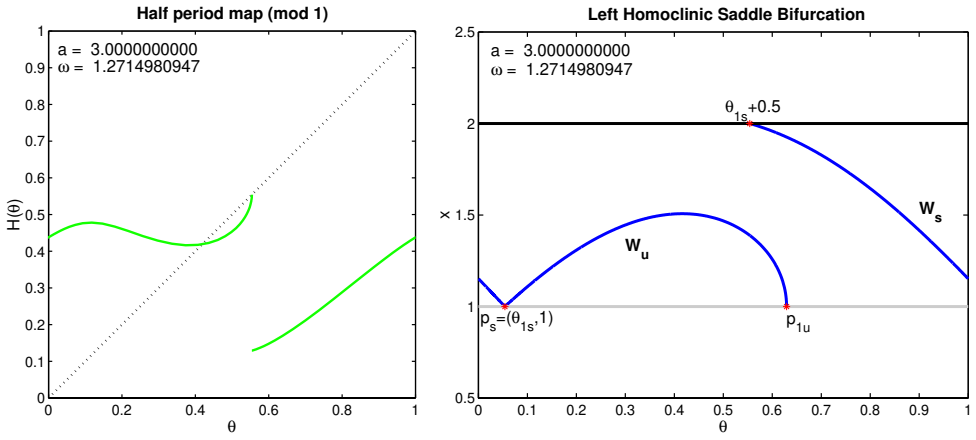

(a) (b)

Figure 5.3. (a) *is a plot of H, and* (b) *illustrates the phase portrait of the orbit at a left homoclinic saddle bifurcation. This bifurcation is apparent in* (a) *since the right end of the first branch of H corresponds to a fixed point.* (b) *shows that the computed orbit satisfies the algebraic condition for a left homoclinic saddle bifurcation $\theta_{2s1} - \theta_{1s} - 0.5 = 0 \pmod 1$.*

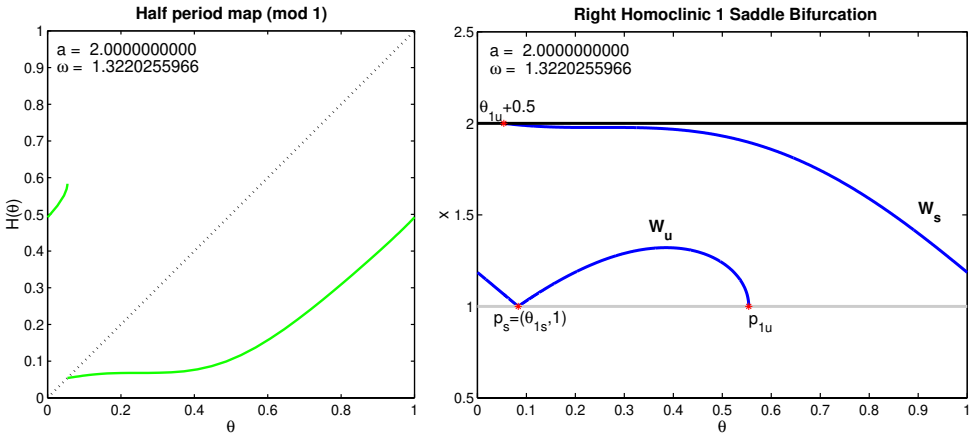

(a) (b)

Figure 5.4. (a) *is a plot of* H*, and* (b) *illustrates the phase portrait of the orbit at a right* 1 *homoclinic saddle bifurcation. This bifurcation is apparent in* (a) *since the left end of the second branch of* H *corresponds to a fixed point.* (b) *shows that the computed orbit satisfies the algebraic condition for a right* 1 *homoclinic saddle bifurcation* $\theta_{2s1} - \theta_{1u} - 0.5 = 0 \pmod 1$.

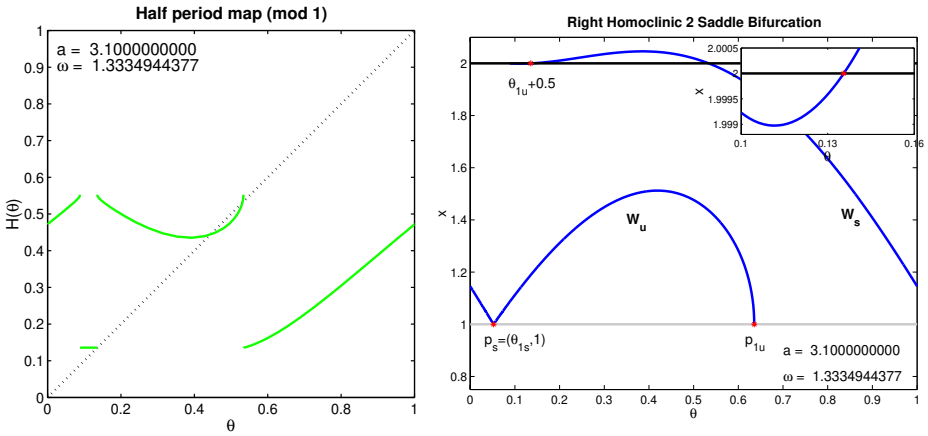

(a) (b)

Figure 5.5. (a) *is a plot of* H*, and* (b) *illustrates the phase portrait of the orbit at a right* 2 *homoclinic saddle bifurcation. This bifurcation is apparent in* (a) *since the right end of the second branch of* H *corresponds to a fixed point. Figure* (b) *shows that the computed orbit satisfies the algebraic condition for a right* 2 *homoclinic saddle bifurcation* $\theta_{2s2} - \theta_{1u} - 0.5 = 0 \pmod 1$.

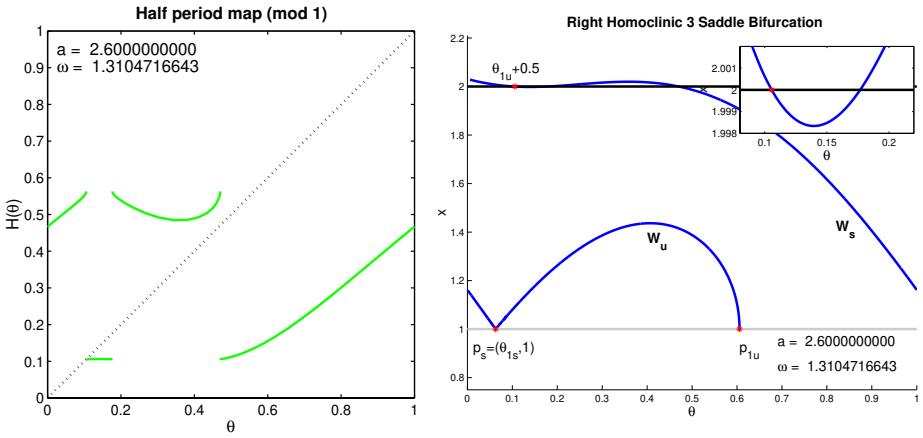

(a) (b)

Figure 5.6. (a) *is a plot of* H*, and* (b) *illustrates the phase portrait of the orbit at a right* 3 *homoclinic saddle bifurcation. This bifurcation is apparent in* (a) *since the left end of the second branch of* H *corresponds to a fixed point.* (b) *shows that the computed orbit satisfies the algebraic condition for a right* 3 *homoclinic saddle bifurcation* $\theta_{2s3} - \theta_{1u} - 0.5 = 0 \pmod 1$*, and the inset shows the last two intersections of the stable manifold* W_s *with the circle* S_2*.*

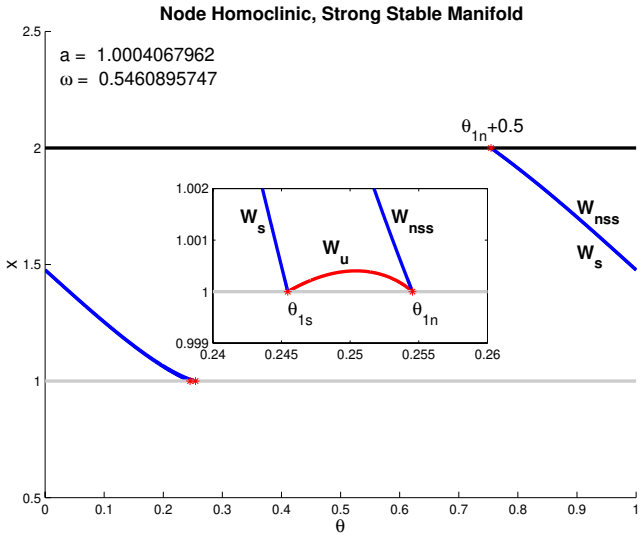

Figure 5.7. *This figure illustrates a nodal homoclinic bifurcation. Note that the computed solution satisfies the algebraic condition* $\theta_{2ss1} - \theta_{1n} - 0.5 = 0 \pmod 1$*. The inset shows the connection between the saddle and the node. We note that it is this same connection that appears in the heteroclinic bifurcations. The plot of the half-return map* H *for these parameter values appears in Figure* 6.3(b).

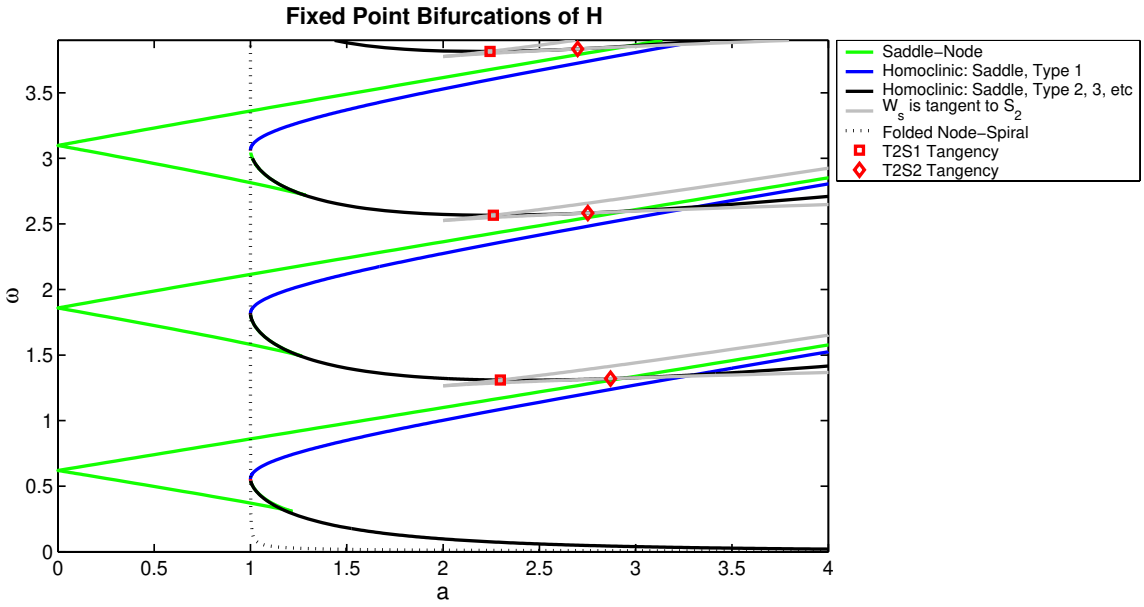

Figure 5.8. *This diagram displays the bifurcation of fixed points of H. The green, blue, and black curves indicate curves of saddle-node points, left homoclinics, and right homoclinics, respectively. The grey curves indicate the parameter values where the stable manifold of the saddle is tangent to the circle S_2. The red squares and red diamonds indicate parameter values where there is a homoclinic orbit and for which the stable manifold of the saddle is also tangent to the circle S_2. Additional features of the diagram that appear on a smaller scale are highlighted in Figures 6.1 and 6.4.*

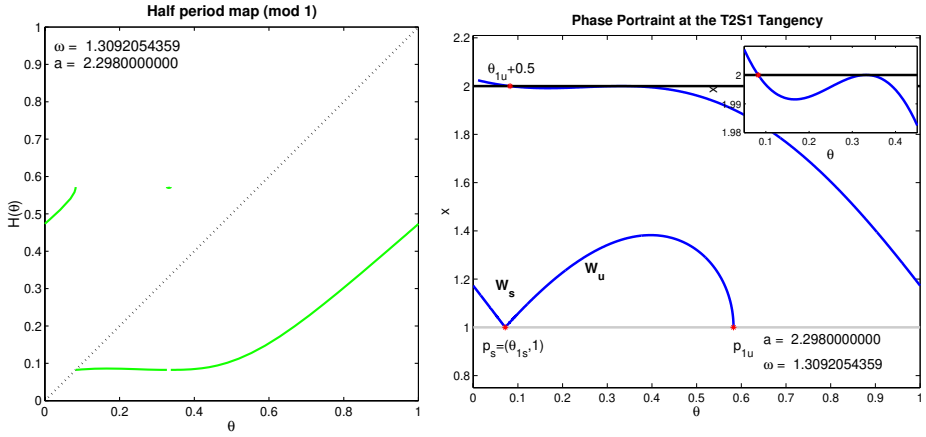

(a) (b)

Figure 5.9. (a) *is a plot of H near a T2S1 tangency, and* (b) *illustrates the phase portrait of the orbit at the same parameter values. The tangency can be seen in the inset of* (b). *Note that the tangency occurs at the first intersection of W_s with $x = 2$.*

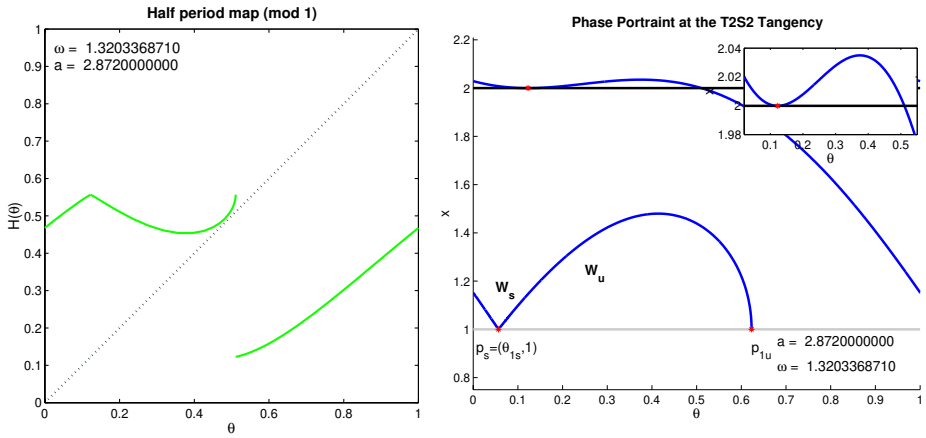

(a) (b)

Figure 5.10. (a) *is a plot of* H *near a* $T2S2$ *tangency, and* (b) *illustrates the phase portrait of the orbit at the same parameter values. The tangency can be seen in the inset of* (b). *Note that the tangency occurs at the second intersection of* W_s *with* $x = 2$.

saddle. Because $(\theta_{2s1}, 2)$ is always a point of S_2 where $x' < 0$, the slope of H is always positive near left homoclinic points. Moreover, the nearby fixed points are unstable since the slope of H is unbounded near the branch ends of Ψ_h orbits that pass to the left of W_s.

Fixed points of H approach a right homoclinic saddle bifurcation if limiting Ψ_h trajectories lie to the right of the stable manifold W_s of the folded saddle (see Figure 5.4). These trajectories then follow the unstable manifold W_u of the saddle and jump to the right of p_{1u}, the intersection of the unstable manifold with $x = 1$. Thus trajectories that approach a right homoclinic saddle bifurcation hit $x = 1$ near θ_{1u} and return to $x = 2$ near the stable manifold of the saddle. The stable manifold W_s may intersect $x = 2$ several times, and the homoclinic point need not jump to the first intersection point. We classify right homoclinic saddle bifurcations by the number of times the stable manifold of the saddle crosses $x = 2$ before returning to the saddle. Thus right homoclinic 1 saddle bifurcations occur when the trajectory returns to $x = 2$ near θ_{2s1}, the first crossing of the stable manifold with $x = 2$. The defining equation for this bifurcation is $\theta_{2s1} - \theta_{1u} - 0.5 = 0 \pmod 1$. Similarly, right homoclinic 2 saddle bifurcations refer to the trajectories that return near the second crossing of the stable manifold with $x = 2$, that is, $\theta_{2s2} - \theta_{1u} - 0.5 = 0 \pmod 1$; an example is shown in Figure 5.5. The only observed right homoclinic saddle bifurcations are of types 1, 2, and 3. Figure 5.6 shows an example of type 3. The analysis of the previous section establishes that the fixed points near a right homoclinic orbit are stable.

Defining equations for the nodal homoclinic bifurcations are such that the intersection of the strong stable manifold of the node with $x = 2$ should have $\theta_{2ss1} = \theta_{1n} - 0.5 \pmod 1$ (see Figure 5.7). Since these bifurcations occur for $a < 2$, the strong stable manifold of the node intersects $x = 2$ only once. Trajectories that lie to the right of the strong stable manifold of the node cross the circle S_1 before approaching the node. Therefore, they make jumps before the trajectories reach the node. Trajectories that lie to the left of the strong stable manifold of the node do not cross the circle S_1. The extension of H to the interval between the

stable manifold of the saddle and the strong stable manifold of the node is constant. For this extended map, the number of fixed points does not change at the nodal bifurcation points, but the fixed points cross from a region where H has positive slope to the extended region, where H is flat.

A qualitative picture of the behavior of H to the right of the strong stable manifold of the folded node can be found by considering the linear flow near a node with an analysis similar to that which we used to determine the slope of H near its branch endpoints. Consider the linear system

$$\begin{aligned}\dot{u} &= -\alpha u,\\ \dot{v} &= -\beta v,\end{aligned}$$

where $\beta > \alpha > 0$. This is a stable node with eigenvectors along the coordinate axes, and the v axis is the strong stable manifold. To obtain a qualitative picture of the behavior of H, we consider a map $u_0 \mapsto u_1$ given by the flow from a line segment $v = v_0$ (and, say, $0 < u_0 < 1$) to the line $v = mu$ (where $m > 0$; this line corresponds to the fold line). The function $u^\beta v^{-\alpha}$ is constant along trajectories; with this we find

$$u_1 = C u_0^{\left(\frac{\beta}{\beta-\alpha}\right)},$$

where $C = \left(\frac{m}{v_0}\right)^{\left(\frac{\alpha}{\beta-\alpha}\right)}$. Thus the map is given by a power law, and since $\beta > \alpha > 0$, the exponent is greater than one. We conclude that the fixed points of H near a nodal homoclinic bifurcation are stable.

5.1.3. Heteroclinic bifurcations. Heteroclinic bifurcations describe curves that are unions of two trajectories that asymptote to both a folded saddle and a folded node. The unstable manifold of the folded saddle lies in the stable manifold of the folded node, giving rise to one segment of the heteroclinic orbit. The second trajectory lies in the stable manifold of the saddle. The defining condition is that the node jumps to the intersection of the stable manifold with S_2. The defining equation is that $\theta_{1n} - \theta_{2s1} - 0.5 = 0 \pmod 1$. Thus the heteroclinic cycle is composed of trajectories lying in the stable and unstable manifolds of the saddle. The primary difference between these bifurcations and the right homoclinics of the saddle is that the unstable manifold W_u approaches the node here, while in the right homoclinic it reaches $x = 1$ and then jumps.

5.2. Description of the bifurcation diagram. Figure 5.8 shows the (numerically computed) bifurcation diagram for fixed points of H in the region $(a, \omega) \in [0, 4] \times [0, 4]$. In this diagram, saddle-node curves are drawn in green, left homoclinic curves in blue, and right homoclinic curves in black. The dotted line separates the region to the right of $a = 1$ with folded nodes from the region with folded foci. The region of the bifurcation diagram close to $a = 1$ will be described in detail in section 6.2 since the bifurcations at $a = 1$ have codimension two.

For $0 < a < 1$, the fixed point bifurcations consist of max and min saddle-node curves, drawn in green. For each circuit number, the min saddle-nodes are the upper branch that appear to extend to infinity. For a sufficiently large, these branches appear to be approximately linear. The lower branch of saddle-nodes in this region are max saddle-nodes. These curves

extend slightly past $a = 1$ but do not extend to infinity as with the curve of min saddle-nodes. We find that these curves end in a cusp that connects to short curves of min saddle-node bifurcation which follow the black curve of right homoclinics back to $a = 1$. This region will be described in more detail in section 6.1.

In the region $a > 1$ and for each circuit number, there are three bifurcation curves that appear to extend to infinity: the min saddle-node bifurcations, the left homoclinic bifurcations, and the right homoclinic bifurcations. Along each right homoclinic curve, two points are marked where the homoclinic orbit is tangent with the line $x = 2$. Changes in the number of intersections of the stable manifold of the saddle with $x = 2$ occur at these locations. The red square separates right saddle homoclinics 1 to the left of the red square from right saddle homoclinics 3 to the right of the red square. See Figure 5.9. The number of crossings switches from 1 to 3 because the stable manifold W_s has a point of tangency with the circle S_2 at the parameter values marked with the red square. To the right of this point along the right saddle homoclinic curve, W_s has 3 crossings of S_2, the third being the homoclinic point. Similarly, the red diamond separates the right saddle homoclinics 3 to its left from the right saddle homoclinics 2 to the right of the red diamond. See Figure 5.10. Here the stable manifold W_s is tangent to the circle S_2 at a local minimum. See Figure 5.10. To the left of the red diamond along the homoclinic curve, the homoclinic points lie to the left of a local minimum in W_s at its second crossing with S_2. To the right of the red diamond along the homoclinic curve, the homoclinic points lie to the right of a local minimum in W_s at its second crossing with S_2.

The types of bifurcations in the bifurcation diagram can be related to properties of the graph of H. The first two crossings of W_s with S_2 bound an interval containing the point $p_{2r} = \frac{1}{2} - \frac{1}{2\pi}\sin^{-1}(\frac{2}{a}, 2)$, where the trajectories of the slow flow have a tangency with S_2 from below. Thus this interval is the branch of H with a local minimum. We call the branch with the local minimum the *central branch* of H. Left homoclinics always occur on the central branch, at its right endpoint. Right homoclinics 2 and right homoclinics 3 occur on the branch immediately to the left of the central branch. In the case of right homoclinics 3, this branch contains the local maximum $\theta_{2l} = \frac{1}{2\pi}\sin^{-1}(\frac{2}{a})$ of H, H has only two branches, and the homoclinic point is the left endpoint of the branch. In the case of right homoclinics 2, the branch is monotonically decreasing and the homoclinic point is the right endpoint of the branch. We also note that, with decreasing ω, new central branches form above the diagonal and then grow in length. Fixed points first appear on the central branch at a min saddle-node bifurcation where the graph of H on the central branch becomes tangent to the diagonal. As ω decreases further, this is quickly followed by a left homoclinic point at which the right endpoint of the central branch crosses the diagonal.

For values of a at which there are folded nodes, there is another curve in the bifurcation diagram corresponding to nodal homoclinic orbits that lie in the strong stable manifold of the folded node. This curve is drawn in magenta on the bifurcation diagram but is sufficiently short that it is difficult to see. Figure 6.4 gives a blown up picture of the region containing the strong nodal homoclinic bifurcation curve on the lowest curve with circuit number 0.

6. Codimension two bifurcations. There are several different points in the bifurcation diagram Figure 5.8 at which bifurcation curves meet or cross. These are codimension two bifurcations of Ψ_h. The previous section discussed tangencies of the stable manifold W_s with

S_2 at right homoclinics where there is no singularity of the bifurcation curve, but its type changes. This section analyzes the remaining codimension two bifurcations of fixed points. We describe each separately and indicate how these bifurcations fit into the diagram of fixed point bifurcations described in the previous section.

6.1. Cusps. Cusps are codimension two bifurcations occurring along the curve of max saddle-node bifurcations. The lower green curve in Figure 6.1 corresponds to the curve of max saddle-nodes that were discussed in the section 5. These curves start at $a = 0$ at the point where the min saddle-node curve meets the max saddle-node curve, and they continue past $a = 1$ to a cusp point just beyond the black curve of right saddle homoclinic orbits (see Figure 6.1). At the cusp, the branch meets a min saddle-node curve that follows the black right homoclinic curve back to $a = 1$. As with the green and blue curves discussed in section 5.2, the location of this curve of saddle-nodes so close to a black curve of homoclinics indicates that these two features are close together in the graph of H. The proximity of these two curves is investigated further in section 6.2. Figure 6.2 shows the half-return map H at a min saddle-node bifurcation on the short branch. Notice that, for nearby parameter values, a homoclinic bifurcation will appear, as can be seen in Figure 6.2.

From the theoretical perspective of singularity theory, we should establish that the fixed point of H has nonzero third derivative at the cusp parameter values. We have not attempted to do this, but the numerical results suggest that this is true.

6.2. Bifurcations at $a = 1$. When $a = 1$, the slow flow has a folded saddle-node equilibrium. At discrete values of ω (one for each circuit number), there is a homoclinic connection along the strong stable manifold of the folded saddle-node. These codimension two points mark the beginning (as a increases) of the more complicated curves of homoclinic points and saddle-node points of H.

In the region of parameter space between $a = 1$ and $a = \sqrt{1 + 1/(16\pi\omega)^2}$, the folded equilibria are saddles and stable nodes. The basin of attraction of the node includes an interval in S_2, and, on this interval, the flow map P_+ is defined to be θ_{1n}, the θ coordinate of the node. Thus the graph of H on this interval is a horizontal line. The left and right endpoints of this interval are the intersections of the stable manifold of the saddle and the strong stable manifold of the node, respectively, with S_2. The value of H on this interval is $\theta_{1n} - \frac{1}{2}$. At the left end of the interval, H has a discontinuity: $\lim_{\theta\to\theta_{2s1}^-} H(\theta) = \theta_{1s} - \frac{1}{2}$, but $\lim_{\theta\to\theta_{2s1}^+} H(\theta) = \theta_{1n} - \frac{1}{2}$.

For each circuit number, there is a region in parameter space between $a = 1$ and $a = \sqrt{1 + 1/(16\pi\omega^2)}$, where the horizontal segment of the graph of H includes a fixed point. If the right end of the interval is a fixed point, there is homoclinic connection along the strong stable manifold of the node. (See Figure 6.3(b).) For circuit number 1, these codimension one points are plotted as a magenta line in Figure 6.4. In this figure, the magenta line ends at the curve $a = \sqrt{1 + 1/(16\pi\omega)^2}$ (the dotted line). Increasing a beyond this point changes the homoclinic point to a fixed point of H (i.e., a periodic orbit of Ψ_h).

If the left end of the interval is a fixed point, there is a heteroclinic connection containing the stable and unstable manifolds of the saddle. (See Figure 6.3(a).) These codimension one points are plotted as a red line in Figure 6.4. At the transition from folded node to

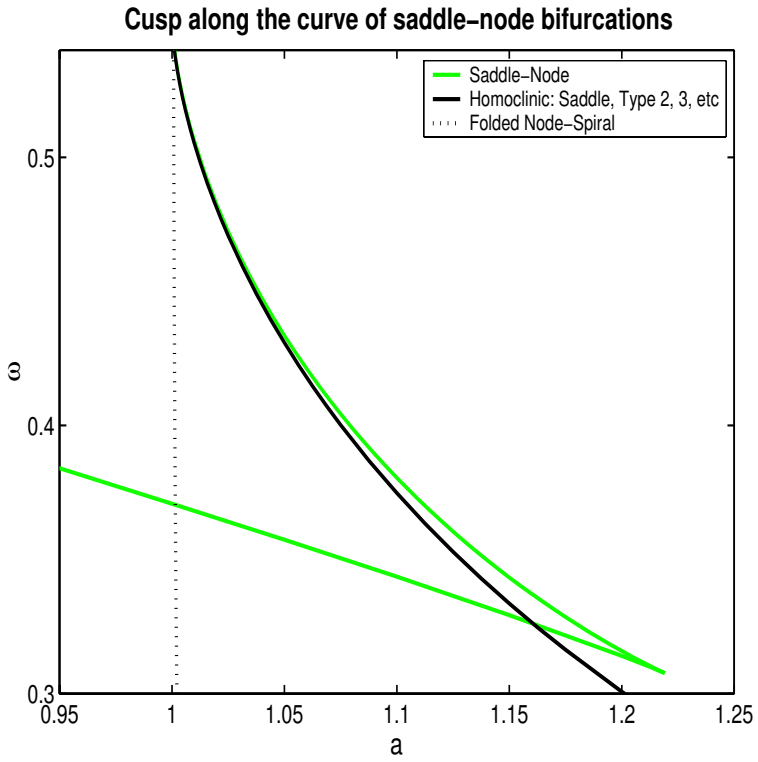

Figure 6.1. *The branches of min saddle-node bifurcations that begin at $a = 0$ continue past $a = 1$ to the cusp shown in this diagram.*

folded spiral, heteroclinic points become right homoclinic points; thus the red curve connects continuously to the black curve in Figure 6.4.

To summarize, the region in parameter space for which the horizontal segment of the graph of H contains a fixed point is the region bounded by the red curve (the heteroclinic points), the magenta curve (the homoclinic points for the strong stable manifold of the node), and the dotted curve (the transition of the stable folded equilibrium from folded node to folded spiral). These curves are shown in Figure 6.4. There are four curves that start at the codimension two point $a = 1$ and $\omega \approx 0.5546$ (where the folded saddle-node has a homoclinic connection). The one upper curve is the blue curve of left saddle homoclinics. There are three lower curves. The lowest curve is the red curve of heteroclinic connections. The middle curve is the magenta curve, where there is a homoclinic connection along the strong stable manifold of the node. Slightly above this curve is the green curve of saddle-node bifurcations. It can be seen in Figure 6.3(b) that only a very small change in the parameters is necessary to perturb the system from the situation of having a stable nodal homoclinic bifurcation to having a saddle-node bifurcation in H. Note that, for values of a smaller than 1, there are no folded equilibria, and the only bifurcations of H are saddle-nodes.

At $a = 1$, the stability of the homoclinic cycles is more subtle to analyze than the stability of the right and left homoclinic cycles because the center manifold of the equilibrium point

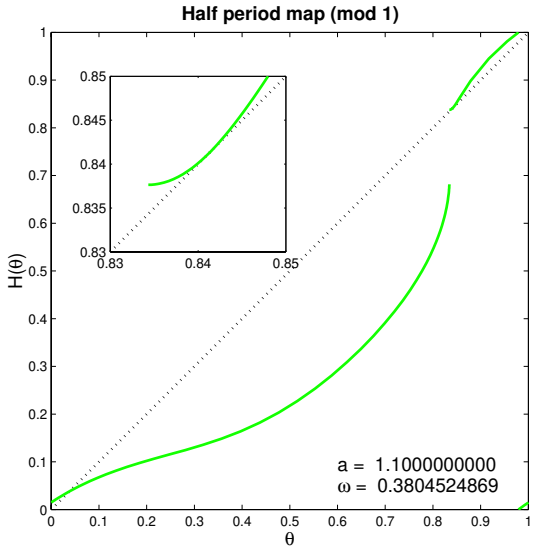

Figure 6.2. *The graph of H at a saddle-node bifurcation point. This point is on the curve of min saddle-node bifurcation shown in Figure 6.1. The inset in the figure shows the tangency of the graph at the point where $H(\theta) = \theta$. It can also be seen that a small change in the parameters can move this to a right homoclinic point, in which the left end of the branch of the graph shown in the inset becomes a fixed point.*

at $(0.25, 1)$ is tangent to the circle S_1. The map from the circle S_2 to the circle S_1 along trajectories adjacent to the strong stable manifold of the equilibrium needs to be determined. We begin with an analysis in normal form of coordinates of a saddle-node that gives most of the information that we need to determine the stability of the map from S_2 to S_1. Consider the (truncated) normal form for a saddle-node equilibrium point of a two-dimensional flow:

$$\begin{aligned} \dot{u} &= u^2, \\ \dot{v} &= -\alpha v. \end{aligned}$$

The solutions of this system are

$$\begin{aligned} u(t) &= \frac{u_0}{1 - tu_0}, \\ v(t) &= v_0 e^{-\alpha t}. \end{aligned} \tag{6.1}$$

We want to compute the map along trajectories from a cross-section of the strong stable manifold to a curve tangent to the center manifold. Take the cross-section to the strong stable manifold to be $v = 1$ and the curve to be the graph of the function $v = h(u)$ with $h(0) = h'(0) = 0$. If the trajectory with initial condition $(u_0, 1)$ flows to (u_1, v_1) with $v_1 = h(u_1)$, then we eliminate t from (6.1) to obtain the implicit equation

$$\exp\left(-\alpha\left(\frac{1}{u_0} - \frac{1}{u_1}\right)\right) = h(u_1),$$

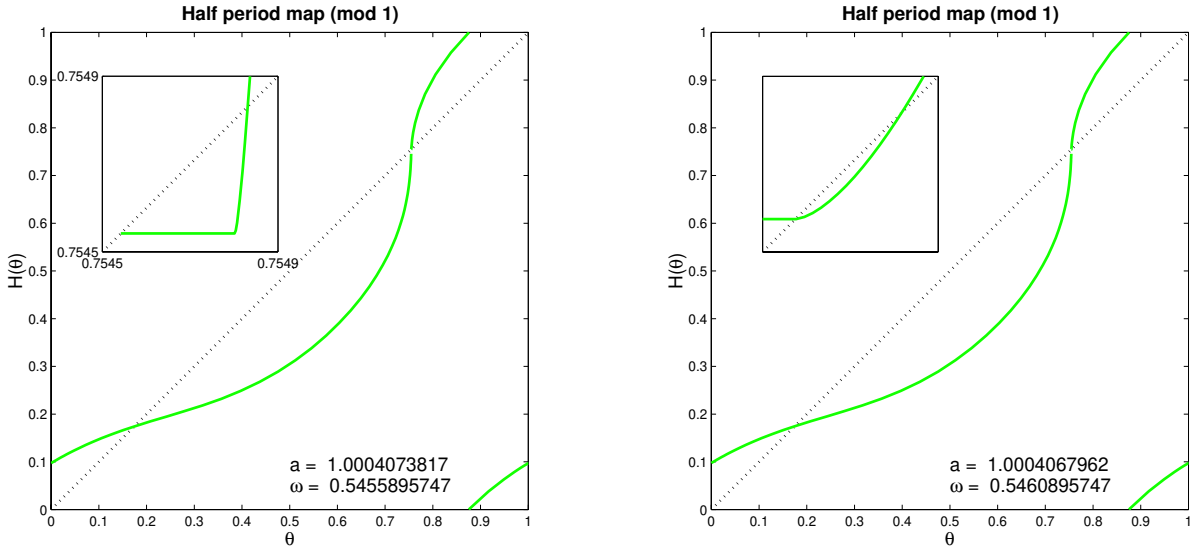

(a) (b)

Figure 6.3. (a) *shows an example of the graph of H when there is a heteroclinic connection. There is a fixed point at the left end of the horizontal segment of the graph of H.* (b) *shows an example when there is a homoclinic connection along the strong stable manifold of the node. The square inset in* (b) *has a width of 5×10^{-7}; the lower intersection of the graph of H with the diagonal dotted line occurs at $\theta \approx 0.754539$. It is clear from this picture that only a very small change in the parameters is required to produce a saddle-node bifurcation in H.*

which can be solved for the inverse of the map along trajectories

$$u_0 = \frac{\alpha u_1}{\alpha - u_1 \ln(h(u_1))}.$$

If $\lim u \ln(h(u)) = 0$ as $u \to 0$, then $\lim \frac{du_0}{du_1} = 1$ as $u_1 \to 0$. This criterion and the tangency conditions are satisfied if $h(u)$ is asymptotic to u^β for some $\beta > 1$.

Now, the center manifold of (3.1) at its saddle-node equilibrium point has quadratic tangency with the curve defined by $x = 1 - 2\pi^2(\theta - 1/4)^2$. This is verified by differentiating this equation and using (3.1) to see that, along the curve,

$$\begin{aligned}(x - 1 + 2\pi^2(\theta - 1/4)^2)' &= -x + \sin(2\pi\theta) + 4\pi^2\omega(\theta - 1/4)(x^2 - 1) \\ &= -(1 - 2\pi^2(\theta - 1/4)^2) + \cos(2\pi(\theta - 1/4) \\ &\qquad + 4\pi^2\omega(\theta - 1/4)(x^2 - 1) \\ &= o((\theta - 1/4)^2)\end{aligned}$$

since $(x^2 - 1) = O((\theta - 1/4)^2)$. We conclude that the slope of the half-return map H approaches a finite slope as θ approaches the strong stable manifold of the saddle-node equilibrium from the right.

We have computed H in a small neighborhood of this strong stable manifold and found that the limit slope is large but finite. At the codimension two point $(\omega, a) = (0.554586, 1)$

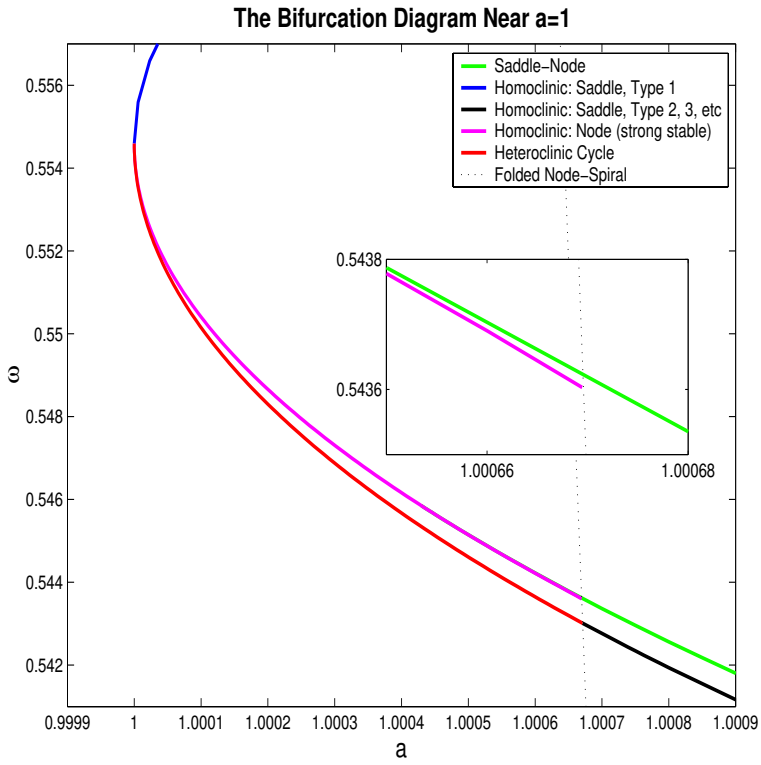

Figure 6.4. *A detail from the bifurcation diagram. This plot shows the curves that emanate from the codimension two point, where there is a homoclinic connection to the folded saddle-node. For circuit number* 0*, this occurs at* $a = 1$ *and* $\omega \approx 0.5546$.

with circuit number 0, the slope is approximately 200. This calculation helps us understand the structure of the bifurcation diagram near $a = 1$. It implies that, for values of a slightly larger than 1, $H' \to 0$ as θ approaches the strong stable manifold of the node from the right but that the slope will increase rapidly and quickly become much larger than one. Thus there will be a local minimum of $H - I$ near the endpoint. (See, for example, Figure 6.3.) When this local minimum of $H - I$ is a fixed point of H, we have a min saddle-node bifurcation. In this regime, there are two intervals in which H has slope smaller than 1 and two intervals in which H has slope larger than 1. As a increases, the intervals which are not adjacent to the discontinuity of H shrink in size, disappearing when there is an inflection point with slope 1. Cusps occur when these inflection points of slope 1 are also fixed points.

6.3. Transversal crossings and the bistable regimes. The simplest codimension two bifurcations for the reduced system are points at which two codimension one bifurcations occur at different places in the phase space. At such points, two codimension one bifurcation curves intersect in the bifurcation diagram. We expect, and find in our numerical computations, that these intersection points are transverse. The crossings play a significant role in the phenomenon of bistability that has been an important part of the history of the forced van der Pol system.

For each value of a larger than those for which cusps occur, the values of ω for which H has a stable fixed point with a given circuit number is an interval bounded below by a right homoclinic curve and bounded above by a point on the curve of min saddle-node bifurcations that originates at $a = 0$. For values of a close to 3, we observe that the min saddle-node curve of circuit number k and the right homoclinic of circuit number $k + 1$ intersect one another transversally. To the right of these intersection points, there are sectors in which there are simultaneously stable fixed points of H with circuit numbers k and $k + 1$. The parameters for which Littlewood [20, 21] deduced the existence of chaotic invariant sets for the flow lie in these regions. To the left of the intersections of min saddle-nodes and right homoclinics, there are regions with no fixed points for H. To the right of these intersection points, H has fixed points for all values of ω. In addition to the two stable fixed points of H, there are also unstable fixed points of H for parameter values just below the min saddle-node curves of circuit number k. These disappear along left homoclinic curves with decreasing ω. We observe that the left homoclinic curve of circuit number k also intersects the right homoclinic curve of circuit number $k + 1$ transversally. In section 7, we show that there is a rich dynamical structure near these codimension two bifurcations, including new families of chaotic invariant sets.

The one additional transversal crossing of bifurcation curves for fixed points that we observe is in the region near $a = 1$, where the max saddle-node curves cross the right homoclinic curves with the same circuit numbers.

7. Period 2 points of H.

Thus far, our discussion of the bifurcation diagram of the forced van der Pol equation has focused on the bifurcations of fixed points of H, the half-return map. In the parameter region $0 \leq a < 1$, the theory of families of circle diffeomorphisms gives a qualitative description of bifurcations of all periodic orbits. Following a brief review of this theory, this section presents a numerical study of periodic orbits of period 2 with circuit number 1. Period 2 orbits are solutions to $H^2(x) = x$. We display graphs of the second iterate H^2 of the half-return map that give insight into the bifurcations of the period 2 orbits. There are many common features between the bifurcations of fixed points and periodic orbits of period 2 for H, but there are significant differences as well. We find new types of codimension two bifurcations involving homoclinic orbits and identify small parameter regimes in which there are new classes of chaotic invariant sets.

7.1. The parameter region $0 \leq a < 1$.

For $0 < a < 1$, the map H is a diffeomorphism of the circle S_2 that varies smoothly with both a and ω. Moreover, the slow flow has a *rotational* property with respect to ω. As ω increases, the direction of the slow flow rotates toward the x axis at a nonzero rate. Since the slow flow is in the sector with decreasing x and increasing ω, two slow flows with the same parameter a and different parameters ω are transverse. These two facts imply that the image of H is strictly increasing with ω. We also conjecture, based upon our numerical computations, that the function $H - I$ appears to have a single local maximum and a single local minimum. This conjecture is sufficient to determine the qualitative properties of the bifurcation diagram in the region $0 < a < 1$ based on the theory of circle diffeomorphisms [1]. There is an *Arnold tongue* of rotation number $\frac{p}{q}$ for each

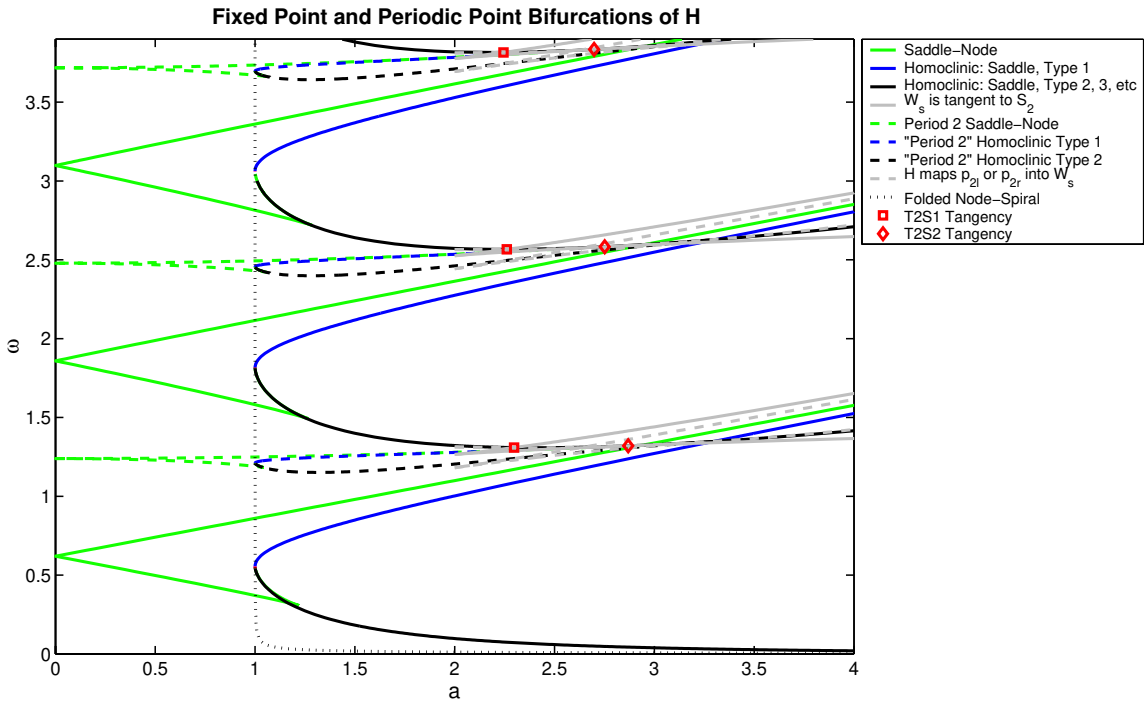

Figure 7.1. *This bifurcation diagram expands the diagram displayed in Figure 5.8 to include the bifurcations associated with period 2 orbits. Note that the same line color is used to distinguish the same types of bifurcation, but the line style indicates whether it is a bifurcation of fixed points or period 2 points.*

rational number $\frac{p}{q}$. This is a strip that begins at[1] $\omega = \frac{2p+q}{(3-2\ln 2)q}$ and intersects each line $0 < a = \text{const} < 1$ in an interval. In the interior of the Arnold tongue, there are two periodic orbits of period q. On the lower boundary of the Arnold tongue, there is a max saddle-node of period q, while on the upper boundary of the Arnold tongue, there is a min saddle-node of period q. For each irrational rotation number ρ and parameter a, there is a single value of ω for which H has rotation number ρ. The set of parameter values with irrational rotation numbers forms a set of positive Lebesgue measure on each line $0 < a = \text{const} < 1$ in the parameter plane.

7.2. An augmented bifurcation diagram. Figure 7.1 is similar to the bifurcation diagram displayed in Figure 5.8 but adds new information about bifurcations of period 2 orbits of H. The bifurcation curves of period 2 orbits are dashed: saddle-node curves are green, left homoclinic curves are blue, and right homoclinic curves are black. Also drawn as gray solid curves are parameters where the stable manifold W_s is tangent to S_2, and gray dashed curves represent parameters where H maps one of the points p_{2l} or p_{2r} into W_s. Figure 7.2 shows the region with period 2 orbits of circuit number 1 in more detail.

[1]When $a = 0$, the slow flow is easily integrated, and we find $H(\theta) = \theta + \omega\left(\frac{3}{2} - \ln 2\right) - \frac{1}{2}$. This is actually the function lifted to the universal cover of S^1; i.e., for the moment, we do not compute H modulo 1. By solving $H^q(\theta) = p$ for relatively prime integers p (the circuit number) and q (the period), we obtain the given formula for ω. The saddle-node curves, in particular, begin at $\omega = \frac{2p+1}{3-2\ln 2}$.

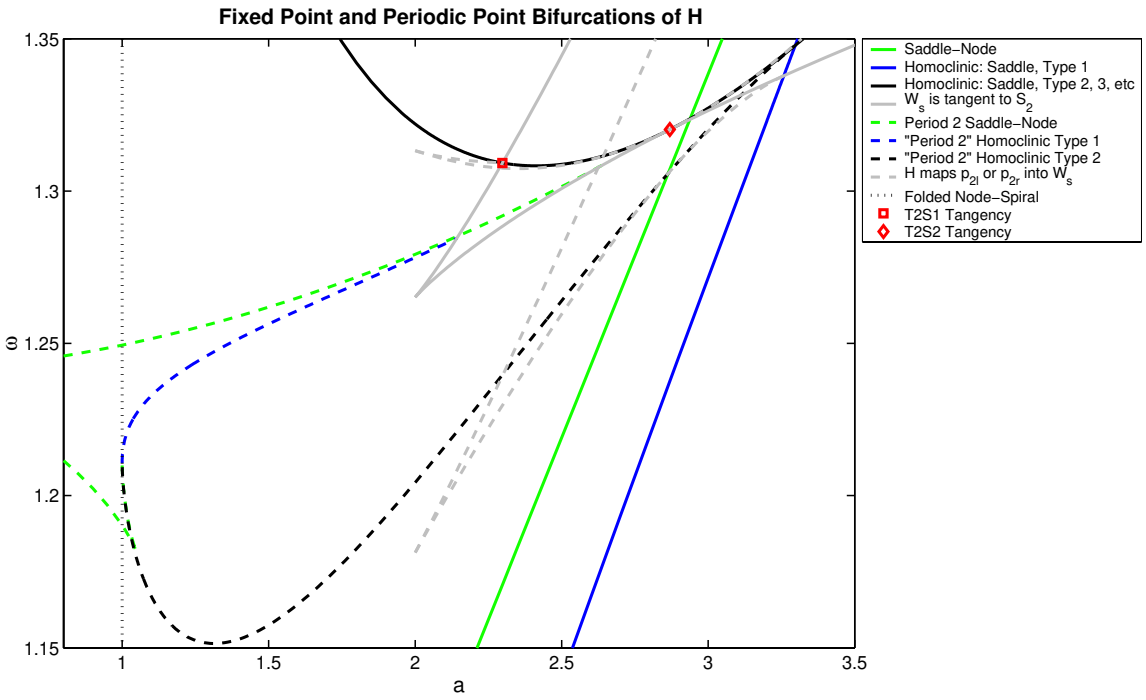

Figure 7.2. *A closer look at part of the bifurcation diagram shown in Figure 7.1.*

Several features of these figures are notable. The gray curves originate at $a = 2$. From each endpoint, two curves emerge that correspond to parameters at which p_{2l} lies in or maps to W_s (lower curves) and parameters at which p_{2r} lies in or maps to W_s (upper curves). "Inside" the solid gray curve, the half-return map H has three points of discontinuity, while outside the cusp it has a single discontinuity. Similarly, the number of discontinuities of H^2 changes as parameters cross the dashed gray curves. The curves where W_s is tangent to S_2 intersect the right homoclinic curves of fixed points at the codimension two points where the type of the right homoclinic curve changes. The intersection at p_{2l}, where the type changes from right homoclinic 3 to right homoclinic 2, is tangential: the tangency curve remains below the right homoclinic curve. There are similar points of tangential intersection along the curves of period 2 right homoclinic bifurcations.

The curve of period 2 min saddle-nodes that begins at $a = 0$ meets the curve of period 2 left homoclinics at a codimension two bifurcation discussed in section 7.3. The curve of period 2 left homoclinics crosses the curve of fixed point right homoclinics. The curves of period 2 left and right homoclinics end at the codimension two bifurcation, where the circuit number 1 right and circuit number 0 left homoclinic curves cross. The coordinates of this point are approximately $(a, \omega) = (3.29725, 1.34783)$. The sequences of bifurcations for the period 2 orbits appear to undergo similar bifurcations to those of the fixed points in the region close to $a = 1$, but we have not explored the bifurcations here thoroughly. Instead, we focus upon the homoclinic bifurcations.

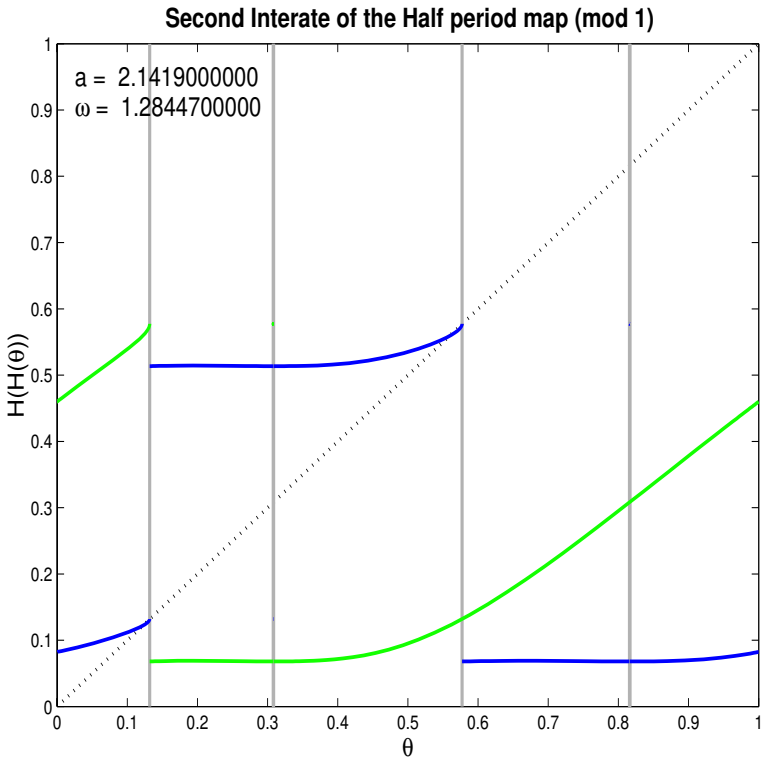

Figure 7.3. *Graphs of H (green) and H^2 (blue) near a point of codimension two bifurcation.*

7.3. Period 2 homoclinic bifurcations. The "morphology" of period 2 homoclinics is substantially more intricate than that of the fixed point homoclinic orbits. In particular, the number of discontinuities of H^2 changes several times along the period 2 homoclinic curves, and there are codimension two bifurcations at which the branches containing the period 2 orbit change. Here we traverse these period 2 homoclinic curves, analyzing the transitions that occur and displaying the graphs of H^2 in different parameter regions.

The upper left homoclinic curve encounters the min tangency curve where the stable manifold of the saddle passes through the point p_{2r} of tangency of the vector field with $x = 2$. The coordinates of the intersection point are approximately $(a, \omega) = (2.14190, 1.28447)$. See Figure 7.3. The map H has three branches for a to the right of the min tangency curve, and the homoclinic point is the third intersection of the stable manifold with $x = 2$. The max tangency curve where the stable manifold of the saddle passes through the point p_{2l} of tangency of the vector field with $x = 2$ crosses the parameter curve where H^2 has a min tangency for $2.62 < a < 2.63$ (i.e., the point p_{2r} maps to the intersection of W^s with $x = 2$.) This has no immediate impact upon the bifurcation curves but creates additional discontinuities of H^2. For example, when $(a, \omega) = (2.63, 1.3084)$, H^2 has eight discontinuities, and its graph has eight branches (see Figure 7.4). For values of a to the right of the max tangency curve, H once again has a single discontinuity.

For (a, ω) near $(2.66384, 1.30982)$, the min saddle-node curve appears to end at parame-

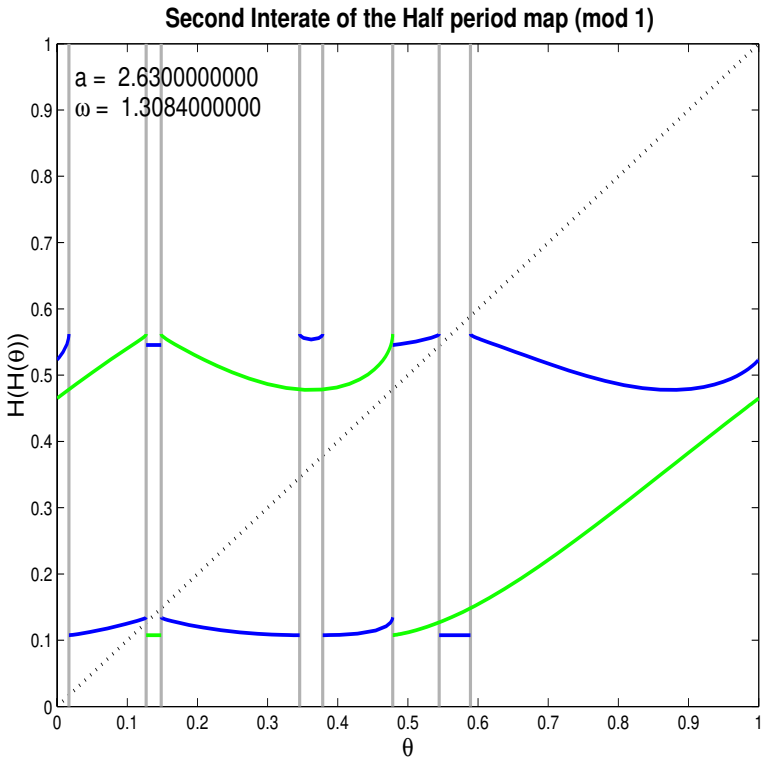

Figure 7.4. *Graphs of H (green) and H^2 (blue) at a point where H^2 has eight branches.*

ters where the left homoclinic curve and the max tangency curve have a point of tangential intersection (see Figure 7.5). Defining equations for this codimension two bifurcation are based upon the conditions that the stable manifold of the saddle passes through p_{2l} and that $H^2(\theta_{2l}) = \theta_{2l}$. The unfolding of the bifurcation depends upon the singularities of H and H^2 at the tangency point. These maps can be modeled as the composition of a quadratic folding map with the power law $|u_1| = |u_0|^{\beta/(\alpha+\beta)}$ as we determined in section 4.2. Thus the composition is the power law $|u_1| = |u_0|^{2\beta/(\alpha+\beta)}$. Since $\beta = \alpha+1$, the exponent is $1+1/(2\alpha+1) > 1$, and the maps H and H^2 have zero derivative at the singularity, which is a local maximum. For values of a smaller than the codimension two point, the homoclinic points lie at the right endpoint of the branch of H^2 to the left of θ_{2l}. This branch has positive slope. For values of a larger than the codimension two point, the homoclinic points lie at the left endpoint of the branch of H^2 to the right of θ_{2l}. This branch has negative slope, so there can no longer be a saddle-node bifurcation of these periodic orbits. Instead, there will be a period-doubling bifurcation curve that lies below (i.e., smaller values of ω) the homoclinic curve. The period-doubling curve affects the stability of the period 2 orbits and signals the presence of period 4 orbits, but new period 2 orbits are not born at the period-doubling bifurcation.

The next codimension two bifurcation along the period 2 left homoclinic curve is its crossing of the period 1 right homoclinic curve at a parameter value $2.79 < a < 2.80$. Here there is simultaneously a fixed point at the left end of the branch of H containing θ_{2l} and a

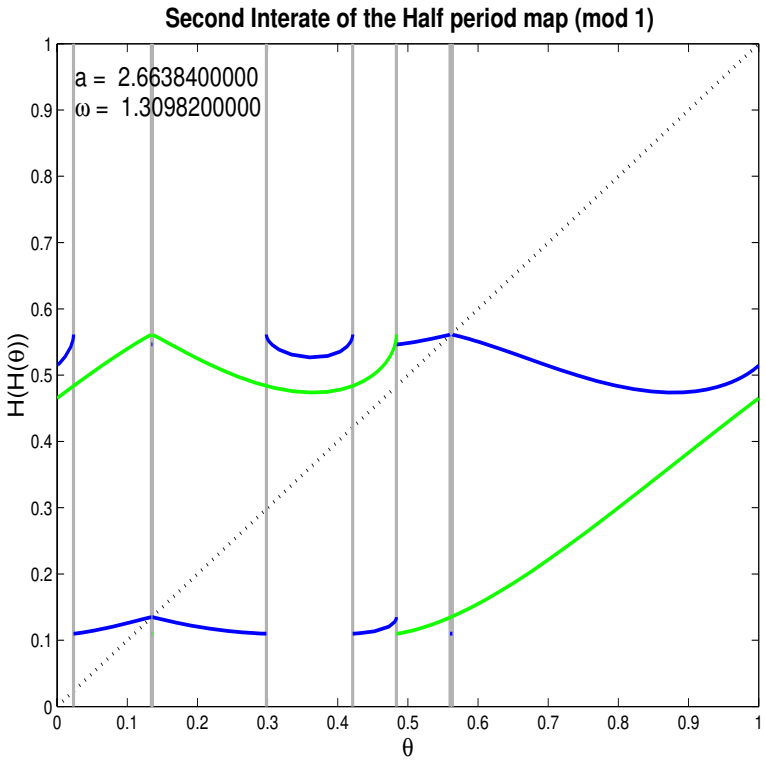

Figure 7.5. *Graphs of H (green) and H^2 (blue) near the end of the min saddle-node curve.*

homoclinic point of H^2 on the branch immediately to the right of the one containing θ_{2l}. For larger values of a, there is a region of bistability with both a fixed point and a period 2 orbit.

The endpoint of the period 2 left homoclinic curve lies at the codimension two point near $(a, \omega) = (3.29725, 1.34782)$, where the right homoclinic curve of fixed points with circuit number 1 crosses the left homoclinic curve of fixed points with circuit number 0 (see Figure 7.6). The period 2 right homoclinic curve also ends at this codimension two point. Apparently, this codimension two point, defined as a transversal crossing of two codimension one bifurcations, is much more complicated than it seems at first glance. Indeed, we find that there are perturbations from this parameter value at which the map H has a chaotic invariant set.

7.4. Chaos without canards. The half-return map H appears to have chaotic trajectories for parameter values $(a, \omega) \approx (3.2, 1.34008531)$. Figure 7.7 shows the graphs of H and H^2, and Figure 7.8 shows detail that illustrates the chaotic invariant set. The parameters $(3.2, 1.34008531)$ are above the left homoclinic curve of fixed points with circuit number 0 and below the right homoclinic curve of fixed points with circuit number 1, in the vicinity of the intersection of these two curves. The branch of H that contains a local minimum has two fixed points—one stable point and an unstable fixed point θ_u close to the right end of the branch. The end of the branch occurs at θ_{2s1}, the first intersection of the stable manifold of the saddle point p_{1l} with $x = 2$. The map H is increasing on $J = [\theta_u, \theta_{2s1})$ with $H(J) = [\theta_u, \theta_r)$. Note that $H(J)$ is bounded on the right by the supremum of H, and on J, H has a single point of

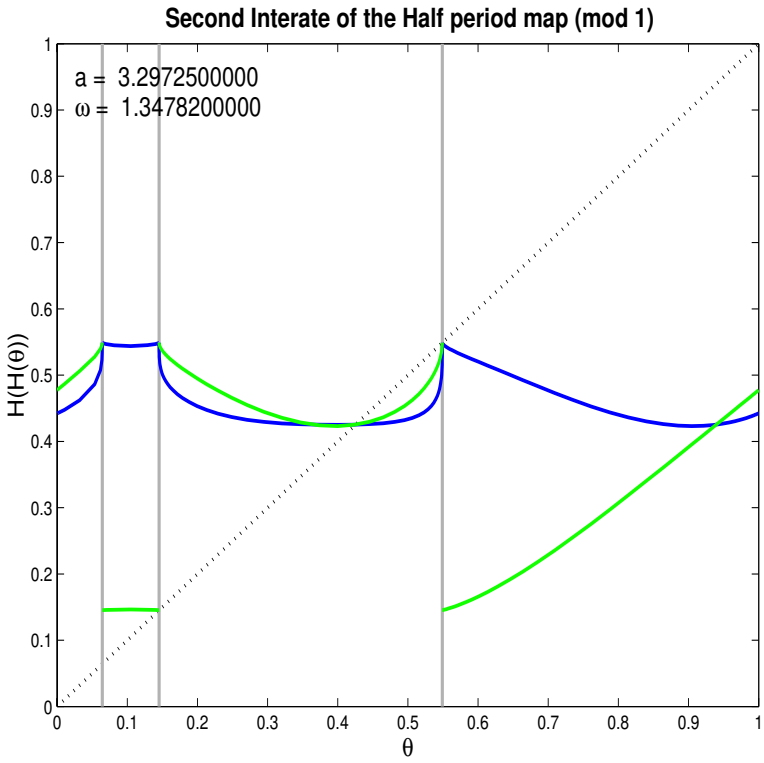

Figure 7.6. *The graphs of H and H^2 at the codimension two point of transversal crossing of right and left homoclinic bifurcations of fixed points.*

discontinuity at θ_{2s1}. We follow the interval $H(J) - J$ for two iterates. First, $H(H(J) - J)$ is an interval whose left endpoint is θ_l, the infimum of H. For the parameter values that lie on a right homoclinic curve of fixed points, θ_l is a homoclinic point of H. For parameter values below this homoclinic curve, $H(\theta_l)$ lies to the right of the discontinuity point θ_{2s2}, inside the branch of H with a local minimum. For parameters near $(a, \omega) = (3.2, 1.34008531)$, the map H is decreasing on $H(H(J) - J)$. We find in numerical calculations that there is a value of $\omega \in (1.34008530, 1.34008531)$ so that $H^2(\theta_r) = \theta_u$, the unstable fixed point. We observe that $H^2(\theta^+_{2s1}) \in H(J) - J$, so $H^2(H(J) - J) \subset H(J)$. We conclude that the union I of the two intervals $H(J)$ and $H(H(J) - J)$ is an invariant set for H. Partitioning I into the three intervals $I_1 = J$, $I_2 = H(J) - J$, and $I_3 = H(H(J) - J)$, we have $H(I_1) = I_1 \cup I_2$, $H(I_2) = I_3$, and $H(I_3) \supset I_1$. This implies that H has a chaotic invariant set that contains a subshift of finite type [27] with transition matrix

$$\begin{pmatrix} 1 & 1 & 0 \\ 0 & 0 & 1 \\ 1 & 0 & 0 \end{pmatrix}.$$

It is quite possible that H not only has a chaotic invariant set for the parameters described above but that I is an attractor. This is true, for example, if the Schwarzian derivative of H on the interval I is negative. Since the map H can be approximated by functions of the form

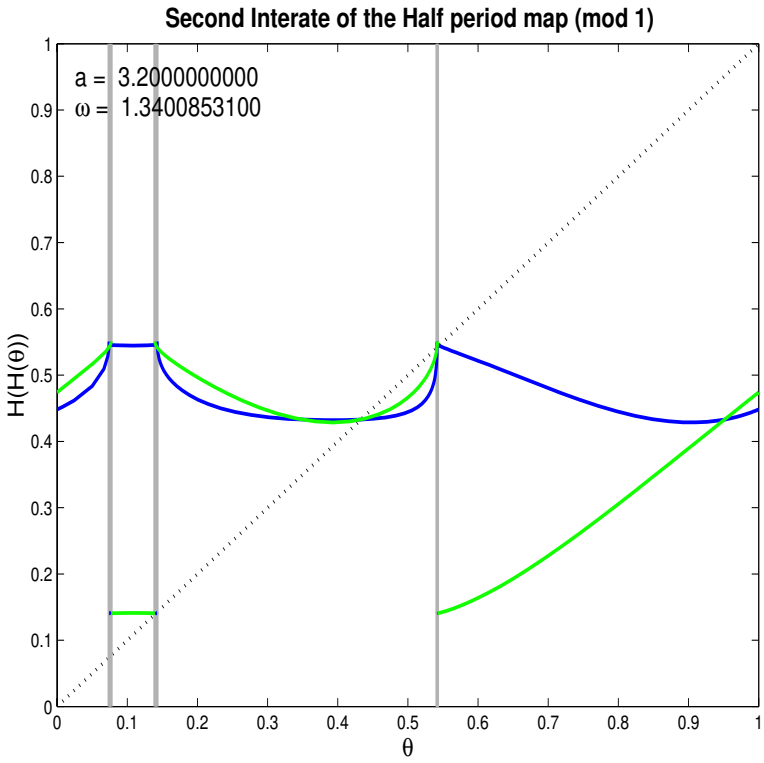

Figure 7.7. *The graphs of H and H^2 at parameters with an apparent chaotic invariant set.*

$f(x) = x^\alpha$ and these functions do have negative Schwarzian derivative, we conjecture that there are parameter values for which H has chaotic attractors. Furthermore, we conjecture that the set of such parameter values has positive measure.

8. Concluding remarks. This section concludes with remarks about

- the methods we used to compute the values of the half-return map H and the bifurcation diagram of the reduced system and
- aspects of the bifurcations of the forced van der Pol equation that are not addressed by the analysis of the slow flow and the reduced system.

Our computations of the half-return map H were performed by numerical integration of the slow flow equations (3.1) from initial conditions on S_2 to their intersection with the circle S_1. We used variable step size Runge–Kutta methods for these integrations, making the error tolerances sufficiently stringent that the apparent errors in the calculations were small enough to produce reliable and robust results. To compute bifurcations of the half-return map H, these numerical integrations were embedded in algorithms that used Newton's method to solve defining equations for each type of bifurcation. For saddle-node bifurcations, the defining equations were obtained by simultaneously solving the fixed point equation $H(\theta) = \theta$ and the equation $H'(\theta) = 1$. For left homoclinic bifurcations, we computed the intersections (θ_{kl}, x_{kl}) of W_s with the line $\theta + 0.5 + k = \theta_{1s}$ in the universal cover of the cylinder $S^1 \times \mathbb{R}$ and then solved the equation $x_{kl} = 2$ using Newton's method. For the right homoclinics, we

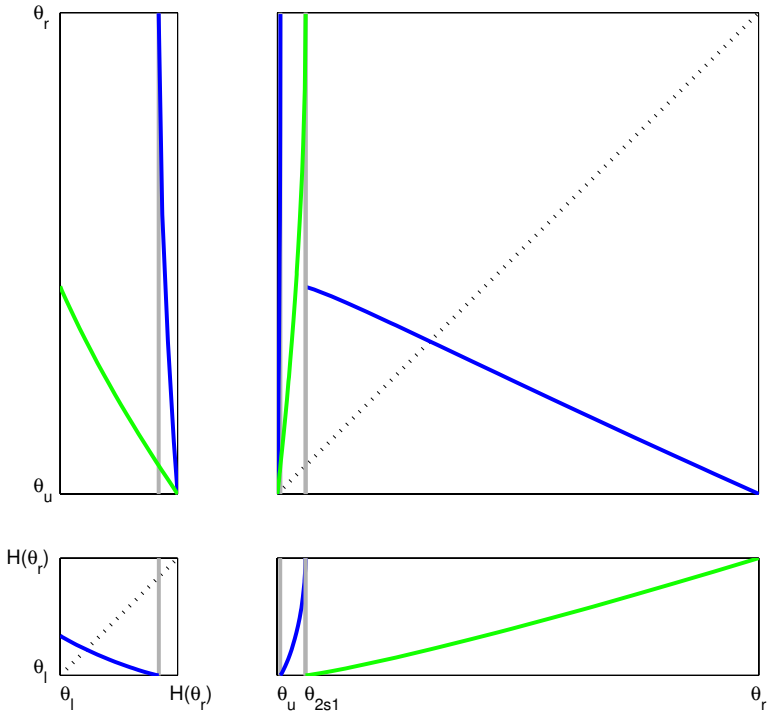

Figure 7.8. *A closer look at H and H^2 for the same parameter values as in Figure 7.7. As in that figure, the green curves are the graph of H, and the blue curves are the graph of H^2. The right interval is $H(J) = [\theta_u, \theta_r]$, and the left interval is $H(H(J) - J) = [\theta_l, H(\theta_r)]$ (where $J = [\theta_u, \theta_{2s1}]$). The union of these two intervals is an invariant set. Its return map consists of the branch of H to the left of the discontinuity and the branch of H^2 to the right of the discontinuity. The coordinate values are $\theta_u \approx 0.541589$, $\theta_{2s1} \approx 0.542117$, $\theta_r \approx 0.550583$, $\theta_l \approx 0.140666$, and $H(\theta_r) \approx 0.142859$.*

computed the intersections (θ_{kr}, x_{kr}) of W_s with the line $\theta + 0.5 + k = \theta_{1u}$ and then solved the equation $x_{kr} = 2$. This procedure of integrating the equation to the desired value of θ and then solving $x = 2$ gave better results than integrating to $x = 2$ because the angles between the vector field and lines of constant θ were much larger than those between the vector field and the lines of constant x at the bifurcation points. This procedure also avoided the necessity of distinguishing the type of right homoclinic to be computed. This was determined after computing the bifurcation point. Similar methods were applied to H^2 to compute the bifurcation curves of period 2 orbits.

The forced van der Pol system is a smooth vector field that does not have discontinuities of its flow. Asymptotic analysis of the behavior of the flow near the folds of its critical manifold is needed to interpret what our results say about bifurcations of the forced van der Pol system. For trajectories that avoid neighborhoods of the folded singularities, classical theory of singularly perturbed systems [2, 19] can be applied for this purpose. However, the analysis of trajectories that pass near the folded singularities is complicated. There even remain gaps in the theory that describes the local geometry of trajectories in the vicinity of the folded nodes [3, 25, 28]. For the global geometry of the flow, there is another level of phenomena

that is not touched upon in this paper. In particular, *canards* are trajectories of the forced van der Pol system that pass near a folded singularity and then continue along the unstable sheet of the critical manifold. These trajectories are not approximated by trajectories of the reduced system as defined here. The canards can be approximated by trajectories of the slow flow that obey different rules about when they jump from one sheet of the slow flow to another, and they give rise to a whole new set of geometric structures in the flow of the forced van der Pol system. The chaotic invariant sets described by Cartwright and Littlewood [8, 9] consist entirely of trajectories that contain canards. The extension of the half-return map to include the canard trajectories, the associated bifurcations, and the existence of horseshoes is addressed in a subsequent paper [4].

REFERENCES

[1] V. Arnold, *Geometrical Methods in the Theory of Ordinary Differential Equations*, Springer-Verlag, New York, 1977.

[2] V. Arnold, V. Afrajmovich, Yu. Ilyashenko, and L. Shil'nikov, *Dynamical Systems* V: *Bifurcation Theory and Catastrophe Theory*, Encyclopaedia Math. Sci., Springer-Verlag, Berlin, 1994.

[3] É. Benoît, *Canards et enlacements*, Inst. Hautes Études Sci. Publ. Math., 72 (1990), pp. 63–91.

[4] K. Bold, C. Edwards, J. Guckenheimer, S. Guharay, K. Hoffman, J. Hubbard, R. Oliva, and W. Weckesser, *The Forced van der Pol Equation* II: *Canards in the Reduced System*, in preparation.

[5] J. Cartwright, V. Eguiluz, E. Hernandez-Garcia, and O. Piro, *Dynamics of elastic excitable media*, Internat. J. Bifur. Chaos Appl. Sci. Engrg., 9 (1999), pp. 2197–2202.

[6] M. L. Cartwright, *Balthazar van der Pol*, J. London Math. Soc., 35 (1960), pp. 367–376.

[7] M. L. Cartwright, *van der Pol's equation for relaxation oscillations*, in Contributions to the Theory of Nonlinear Oscillations II, Princeton Ann. Math. Stud. 2, Princeton University Press, Princeton, NJ, 1952, pp. 3–18.

[8] M. Cartwright and J. Littlewood, *On nonlinear differential equations of the second order* I: *The equation* $\ddot{y} - k(1-y^2)\dot{y} + y = bk\cos(\lambda t + a)$, *k large*, J. London Math. Soc., 20 (1945), pp. 180–189.

[9] M. Cartwright and J. Littlewood, *On nonlinear differential equations of the second order* II: *The equation* $\ddot{y} - kf(y,\dot{y})\dot{y} + g(y,k) = p(t) = p_1(t) + kp_2(t)$, $k > 0$, $f(y) \geq 1$, Ann. of Math. (2), 48 (1947), pp. 472–494.

[10] M. Cartwright and J. Littlewood, *Addendum to "On nonlinear differential equations of the second order* II, Ann. of Math. (2), 50 (1949), pp.,504–505.

[11] N. Fenichel, *Persistence and smoothness of invariant manifolds for flows*, Indiana Univ. Math. J., 21 (1971), pp. 193–225.

[12] R. FitzHugh, *Impulses and physiological states in models of nerve membrane*, Biophysics J., 1 (1961), pp. 445–466.

[13] J. Flaherty and F. Hoppensteadt, *Frequency entrainment of a forced van der Pol oscillator*, Stud. Appl. Math., 58 (1978), pp. 5–15.

[14] J. Grasman, *Asymptotic Methods for Relaxation Oscillations and Applications*, Springer-Verlag, New York, 1987.

[15] J. Guckenheimer, K. Hoffman, and W. Weckesser, *Numerical computation of canards*, Internat. J. Bifur. Chaos Appl. Sci. Engrg., 10 (2000), pp. 2669–2687.

[16] J. Keener, *Chaotic behavior in a piecewise continuous difference equation*, Trans. Amer. Math. Soc., 261 (1980), pp. 589–604.

[17] M. Levi, *Qualitative analysis of the periodically forced relaxation oscillations*, Mem. Amer. Math. Soc., 244 (1981), pp. 1–147.

[18] C. Koch and I. Segev, *Methods in Neuronal Modeling*, MIT Press, Cambridge, MA, 1998.

[19] N. Levinson, *A second order differential equation with singular solutions*, Ann. of Math. (2), 50 (1949), pp. 127–153.

[20] J. Littlewood, *On nonlinear differential equations of the second order* III: *The equation* $\ddot{y} - k(1-y^2)\dot{y} + y = bk\cos(\lambda t + a)$ *for large* k *and its generalizations*, Acta Math., 97 (1957), pp. 267–308 (errata in Acta. Math., 98 (1957), p. 110).

[21] J. Littlewood, *On nonlinear differential equations of the second order* IV: *The equation* $\ddot{y} - kf(y)\dot{y} + g(y) = bkp(\phi), \phi = t + a$ *for large* k *and its generalizations*, Acta Math., 98 (1957), pp. 1–110.

[22] S. McMurran and J. Tattersall, *The mathematical collaboration of M. L. Cartwright and J. E. Littlewood*, Amer. Math. Monthly, 103 (1996), pp. 833–845.

[23] R. Mettin, U. Parlitz, and W. Lauterborn, *Bifurcation structure of the driven van der Pol oscillator*, Internat. J. Bifur. Chaos Appl. Sci. Engrg., 3 (1993), pp. 1529–1555.

[24] E. Mischenko and N. Rozov, *Differential Equations with Small Parameters and Relaxation Oscillations*, Plenum Press, New York, 1980.

[25] E. Mischenko, Yu. Kolesov, A. Kolesov, and N. Rozov, *Asymptotic Methods in Singularly Perturbed Systems*, Consultants Bureau, New York, 1994 (translated from the Russian by Irene Aleksanova).

[26] P. F. Rowat and A. I. Selverston, *Modeling the gastric mill central pattern generator of the lobster with a relaxation-oscillator network*, J. Neurophysiology, 70 (1993), pp. 1030–1053.

[27] S. Smale, *Diffeomorphism with many periodic points*, in Differential and Combinatorial Topology, S. Cairns, ed., Princeton University Press, Princeton, NJ, 1963, pp. 63–80.

[28] P. Szmolyan and M. Wechselberger, *Canards in* R^3, J. Differential Equations, 177 (2001), pp. 419–453.

[29] F. L. H. M. Stumpers, *Balth. van der Pol's work on nonlinear circuits*, IRE Trans. Circuit Theory, 7 (1960), pp. 366–367.

[30] F. Takens, *Forced oscillations and bifurcations*, Comm. Math. Inst. Rijkuniv. Utrecht, 3 (1974), pp. 1–59.

[31] F. Takens, *Constrained Equations: A Study of Implicit Differential Equations and Their Discontinuous Solutions*, Report ZW-75-03, Mathematisch Institut, Rijksuniversiteit, Groningen, The Netherlands, 1975.

[32] B. van der Pol, *A theory of the amplitude of free and forced triode vibrations*, Radio Review, 1 (1920), pp. 701–710, 754–762.

[33] B. van der Pol, *On "Relaxation Oscillations"* I, Phil. Mag., 2 (1926), pp. 978–992.

[34] B. van der Pol, *The nonlinear theory of electric oscillations*, Proc. IRE, 22 (1934), pp. 1051–1086.

[35] B. van der Pol and J. van der Mark, *Frequency demultiplication*, Nature, 120 (1927), pp. 363–364.